

Sloshing in High Speed Galaxy Interactions

Thomas Zeltwanger

University of Maine

Department of Physics and Astronomy, 5709 Bennett Hall, Orono, ME 04469

kickers@email.com

Neil F. Comins

University of Maine

Department of Physics and Astronomy, 5709 Bennett Hall, Orono, ME 04469

neil.comins@umit.maine.edu

and

Richard V. E. Lovelace

Cornell University, Department of Astronomy, Ithaca, NY, 14853

rvl1@Cornell.edu

Received _____; accepted _____

ABSTRACT

Observations of lopsided spiral galaxies motivated us to explore whether the rapid passage of a companion galaxy could cause them. We examine whether the center of mass of the visible matter becomes displaced from the center of mass of the dark halo during the intruder's passage, thereby causing an asymmetric response and asymmetric structure. Two dimensional N -body simulations indicate that this can happen.

We also explore some consequences of this offset. These include the center of mass of the visible disk following a decaying orbit around the halo center of mass and the development of transient one-armed spirals that persist for up to six rotation periods.

We then study the results of a variety of initial conditions based on such offsets. We report on the results of several runs in which we initially offset a disk from its halo's center of mass by an amount typical of the above interaction. In some runs the halo is free to move, while in others it is held fixed. We used three different mass distributions for the halo in these runs. We find that the disk's center of mass spiraled inward creating a variety of observed or observable phenomena including one-armed spirals, massive clumps of particles, and counter-rotating waves. The systems settle into relatively axisymmetric configurations. Whether or not the end states included a bar depended on a variety of initial conditions.

Subject headings: galaxies: interactions — galaxies: spiral — methods: n-body simulations

1. INTRODUCTION

Several groups have reported observations of lopsided H I (Baldwin, Lynden-Bell, & Sancisi 1980; Richter & Sancisi 1994) and stellar distributions (Lauer et al. 1993, 1996; Rix & Zaritsky 1995; Davidge et al. 1997; Zaritsky & Rix 1997; Conselice 1997) in a significant fraction of spiral galaxies. The percentage of galaxies that are measurably lopsided range from 30% of field spirals (Zaritsky & Rix 1997; Kornreich et al. 1998) to 50% of all spiral galaxies (Swaters et al. 1999). These numbers may be high if, as proposed by Zaritsky & Rix (1997), lopsided galaxies are brighter than symmetric galaxies, thereby biasing the statistics. Nevertheless, a significant number of lopsided galaxies are observed. These findings have prompted a number of papers exploring the origins and dynamics of these asymmetries.

Baldwin, Lynden-Bell, & Sancisi (1980) proposed a simple kinematic model for lopsided galaxies in which different rings of the galaxy, assumed non-interacting, are initially shifted from their centered equilibrium positions. The shifted rings precess in the overall gravitational potential in a direction opposite to that of the mass motion. Because the precession rate decreases in general with radial distance, an initial disturbance tends to “wind up” into a leading spiral arm in a time appreciably less than the Hubble time. Miller & Smith (1988, 1992) have made extensive computer simulation studies of the unstable eccentric motion of matter in the nuclei of galaxies, which they suggest is pertinent to the off-center nuclei observed in a number of galaxies such as M31, M33, and M101.

More recent ideas on the origin of lopsidedness include galaxy mergers (Zaritsky & Rix 1997), and counter-rotating matter (Sellwood & Merritt 1994). Schoenmakers, Franx, & de Zeeuw (1997) interpret optical asymmetry as an indicator of asymmetry in the overall galactic potential and therefore an indicator of the spatial distribution of the dark matter in a galaxy, which may have a triaxial distribution. By analyzing the spiral components

present in the surface brightness or H I distribution, the velocity gradient, and therefore, the shape of the gravitational potential, may be uncovered. Jog (1997) studied the orbits of stars and gas in lopsided potentials and concluded that a stationary lopsided disk may indicate asymmetry in the halo.

A further possibility is that an optical disk may be in a quasi-stationary lopsided state in a symmetric potential, as discussed by Syer & Tremaine (1996). In this model, gaseous and stellar matter that is not fully relaxed swirl about the minimum of the halo potential. The result is a lopsided flow within a symmetric mass distribution. Numerical simulations of this situation have been done by Levine & Sparke (1998) using a gravitational N -body tree-code method for disk galaxies shifted from the center of the main halo potential. The results are suggestive of lopsidedness with large lifetimes.

An N -body simulation study of a rotating spheroidal stellar system including the dynamics of a massive central object by Taga & Iye (1998a) indicates that the central object goes into a long lasting oscillation similar to those found earlier by Miller & Smith (1988, 1992) and which may explain asymmetric structures observed in M31 and NGC 4486B. A linear stability analysis of a self-gravitating fluid disk with a massive central object also by Taga & Iye (1998b) indicates a linear instability (Taga & Iye 1998b). A study of the eccentric motion of a disk galaxy made up of a large number of self-gravitating rings shows instability in the inner part of the disk (< 2 kpc) and the excitation of long lasting trailing one armed spiral waves (Lovelace et al. 1999).

In this paper we explore two issues surrounding lopsided galaxies. First we examine the gravitational response of an N -body disk galaxy model embedded in a halo to the high speed passage of a companion galaxy. Then, assuming that a disk galaxy has been perturbed by a passing galaxy or other mechanism, we explore the response of the system to a variety of displacements and relative velocities of a disk of stars offset from their halo

centers of mass. In some of these runs, we have both the stars and halo free to move, while the halo is fixed in the remaining runs. We report on runs with different initial conditions and different mass distributions.

We use our two dimensional N -body GALAXY code (Schroeder & Comins 1989; Schroeder 1989; Shorey 1996), with 100,000 collisionless particles representing stars (or perhaps more properly, galactic clusters) and a gravitating halo that comprises 75% of the system's total mass. One of our goals is to determine how perturbations, such as the passage of a companion galaxy or offset halo-disk centers of mass, affect the formation and evolution of bars in galaxies. A sufficiently massive halo will quickly dampen almost any bar (Binney & Tremaine 1987; Sellwood 1983). We have therefore chosen this 75% halo because it has insufficient mass to suppress the development of a bar that may be driven into existence during the run (Comins et al. 1997). The halos we use are sufficiently massive, however, to simulate the gravitational effect of a significant dark matter galactic component. We therefore expect that the suppression of any bar that develops and decays in our runs would be due to the dynamics that the disk undergoes.

Both the creation and the destruction of bars have been discussed by several groups. Noguchi (1996) proposed that bars in late-type galaxies have intrinsic origins, while bars in early-type galaxies have been formed by tidal interactions with other galaxies. Specifically, Miwa & Noguchi (1998) found that tidal effects due to a close encounter between galaxies may trigger the formation of a bar in an otherwise barstable disk. Athanassoula (1996a,b, 1999) performed N -body simulations of the interactions of a barred disk galaxy with a close companion galaxy. She found that the bar may be destroyed as a consequence of this interaction, or that an offcentered bar may form. The destruction of the bar occurs most likely in the case of a merger, when most of the companion reaches the target's center.

The initial particle velocity distribution in each run is determined by Q_0 , the initial

value of Toomre’s Q . We chose to set Q_0 to a marginally stable $Q_0 = 1.1$ over the entire disk. The offset runs lasted just under 10 rotation periods, as measured at the half-mass radius of the disk. The particles initially form a counter-clockwise rotating disk.

The simulation is done on a Cartesian grid with 256×256 cells. During the runs with the intruder present, the test galaxy and its halo had a diameter of 128 cells. To maximize use of computer memory and time, the intruder galaxy was a point particle, sent into a coplanar orbit. The perigalactic distance between the two galaxies was chosen so that they would not overlap even if they both had realistic radii. This precludes any dynamical friction between them. Their minimum separation was 42 cell widths and the intruder was on the grid for less than one rotation period of the test galaxy.

During the runs without the intruder, the test galaxy’s initial diameter is enlarged to 192 cells. This enables us to more accurately simulate small-scale features. For a typical disk galaxy of radius 10 kpc (Binney & Tremaine 1987) this translates into a cell width of roughly 104 pc. Each rotation period of the disk corresponds to roughly 250 Myr.

Runs were made with three different halo mass distributions:

1. The distribution, as described by Sellwood & Carlberg (1984) and Carlberg & Freedman (1985), that creates a rotation curve simulating that of an Sc galaxy.
2. The isothermal distribution described in Binney & Tremaine (1987).
3. An isothermal distribution plus the gravitational potential of a supermassive central black hole.

The rotation curves for these potentials are all presented together in Figure 1.

Tables 1, 2, and 3 list the basic properties and results for these runs. Column 1 in each of these tables lists the run numbers referred to throughout the paper. All runs used an Sc

distribution for the disk.

In §2 we present the results of 5 runs in which an intruder galaxy passes the target galaxy. In §3 we present the results of 12 runs in which the stars and halo initially have different centers of mass, along with three reference runs with the same mass distributions and no initial offsets. In §4 we compare these runs to each other, to previous simulations, and to observations that they may explain. In §5 we present our conclusions.

2. EFFECTS OF A HIGH SPEED GALACTIC COLLISION

Disk galaxies interacting with neighboring galaxies have lopsided structures as seen, for example, in Karachentsev 64 and M101. Unlike simulations of slow-speed interactions that lead to mergers (Hernquist & Mihos 1995; Zaritsky & Rix 1997), we send a simulated companion in a high speed, slightly positive-energy, coplanar orbit that takes it past the target galaxy and off the grid. The intruder is modeled as a point mass with 20% the total (halo plus disk) mass of the target galaxy. It is initially sent onto the grid passing the target galaxy in the same direction as the target galaxy’s star particles orbit. The intruder enters at an angle adjusted so that, even if it did have a realistic distribution of stars, it would not collide with the target galaxy. This prevents the merger of the two galaxies, which we do not seek to simulate.

The first two intruder runs had the halo simulated by a second *N*-Body component of 10000 particles with a different Q than the star particles. Therefore, both the star and halo particles responded to the gravitational influence of the intruder, as well as to each other. (Halos that move we denote as dynamic, while fixed halos are called static.) One of these runs (hereafter Run 1) simulated a dynamic halo of cold matter, with an initial $Q_{0,halo} = 0.3$. The other run (Run 2) simulated a dynamic halo of hot matter, with

$$Q_{0,halo} = 5.0.$$

Figure 2 shows the displacement of the center of mass motion of the stars relative to the center of mass of the halo in Run 1. The halo’s center of mass is always located at (0.0,0.0) in this, and similar, figures. The maximum separation between the halo and star centers of mass is three quarters of a cell width (78 pc). Although “noisy”, Figure 2 shows distinct periodic, cyclic motion as the two centers of mass waltz around each other. The dynamics of this run are complicated by the fact that the cold halo particles develop a bar, which persists throughout the $6\frac{1}{4}$ rotation periods of the run.

Figure 3 shows the separation in Run 2 between the stellar and halo centers of mass as. This is the hot halo case. Due to the greater kinetic energy in its particles, we expect that the halo center of mass will be displaced less than the stars in this run. This is what we observe. As a result, the maximum separation is nearly two grid cells or 208 pc. No bar develops in this halo.

Next we ran three intruder runs with a hydrodynamic simulation of the halo. These were done to avoid the effects of dynamic friction that were observed to occur between the star and halo particles (each with initially different Q_0) in Runs 1 and 2. We used an Sc mass distribution of compressible, shockable, gravitating gas. Instead of assigning an initial Q , we give the gas an initial uniform energy density. This is equivalent to giving the gas a temperature profile.

Figure 4 shows the center of mass separations between the halo and stars for the case with a low initial energy density gas corresponding to an initial gas temperature of $T_0 = 0.5$ K as measured at the half mass radius. During the run, denoted Run 3, the maximum separation between the halo and star centers of mass reached nearly 3 cell widths or 312 pc. The result for the $T_0 = 5.0$ K run (Run 4) is similar with a maximum separation of nearly 6 cell widths.

The results of the hottest gas run (Run 5), with $T_0 = 5 \times 10^5$ K, are especially intriguing. Figures 5 and 6 show the gas and star distributions throughout this run. Note that in this and all other intruder runs, the intruder travels counterclockwise, entering the grid at roughly the 5 o'clock position and leaves at roughly the 1 o'clock position at time $t = 0.98$ rotation periods. After leaving the grid, the intruder's gravitational potential is ignored. In response to the intruder, a bulge is clearly visible at the three o'clock position in both the gas and stars at time 0.861 rotation periods. Note the similarity between timestep 4.898 in Figures 5 and 6 and the optical image of Karachentsev 64 (Figure 7). Karachentsev 64 is a pair of interacting spiral galaxies.

The centers of mass of both components drift upward throughout this run. This is due to the asymmetry created in the spiral arms by the intruder's passage. The more open arm, on the left, carries angular momentum downward and to conserve it, the rest of the system moves upward. The relative displacement between the centers of mass in this run is shown in Figure 8. While the dynamics of the system greatly complicate the relative center of mass motion, clearly it still exists.

Because of the differences in behaviors of particles and gas acting as the halo, these three gas halo runs cannot be compared directly with the previous two N -body halo runs. Nevertheless, the behavior of all five consistently show an offset between the two centers of mass. Furthermore, the “hotter” the halo, the greater the offset.

In all of our runs, the center of mass of the stellar disk moves relative to the center of mass of its halo as a result of the gravitational interaction with an intruder. This provides the motivation to explore the dynamics of visible matter sloshing around in a deep gravitational halo. The difficulties with doing this following the perturbation of an intruder, as in Runs 1 through 5, are two-fold. First, as we saw in Run 5, the transients created by the intruder's extremely powerful and asymmetric passage make it difficult to

see how the star system is responding just to its halo’s potential. Second, there may be other mechanisms that cause a separation of centers of mass that are not so disturbing to the system. Therefore, we now look at systems with initial offsets between the star and halo centers of mass, but without any intruder to mix up the system.

3. OFFSET RUNS

3.1. Dynamic Halo Runs

We proceed now by displacing a variety of stellar disks from the centers of mass of their halos. Our first four offset runs, labeled Runs 6 – 9, have both stars and halo free to move. Predictably, the two runs with dynamic N -body halos show significant dynamical friction between the stars and halo particles. These lead to rapid damping of the center of mass motion. In the low angular momentum Run 6, the stars and halo have essentially the same centers of mass and are in equilibrium configurations within less than four rotation periods. The relative positions of the centers of mass show little, if any, periodic motion during the run (Figure 9).

Transient structure occurs in the stars in Run 6. They evolve a multiarmed spiral pattern which changes to a two-armed spiral and then to a symmetric disk by the beginning of the fourth rotation period. This is also a typical evolution of a non-offset N -body system moving in the potential of a fixed halo. In comparison, the transient structures seen in the high angular momentum version, Run 7, shows a significant feathery one-armed spiral structure that evolves to a small bar with a ring surrounding it and then to a symmetric system, after less than four rotation periods (Figure 10). Similar one-arm features have been reported by Lotan-Luban (1990), as mentioned in Struck (1999), in head-on, low impact parameter collisions. The center of mass of the stars in our Run 7 follow an arc

inward, damped after 1.8 rotation periods by the dynamical friction, again with little indication of periodic motion relative to the halo’s center of mass.

If, as seems likely, most of the true halo mass is a smoother distribution of matter, less prone to the effects of dynamical friction, it would be more appropriate to simulate it’s dynamic behavior by that of a gravitating fluid. Therefore, we made two runs with our gravitating gas component serving as the halo, as in Runs 3 – 5, above. Run 8 has the same initial conditions as Run 6: hot halo, large initial center of mass offset, and small initial angular momentum for the stars.

Both the halo gas and the stars in Run 8 go through non-axisymmetric transients. After about $1\frac{3}{4}$ rotation periods, the gas settles into a two-armed spiral structure. The stars develop a distinct bar with spiral arms winding out from its ends. The spiral structure is much more distinct in the gas than in the star particle component (Figures 11a and 11b).

Unlike the runs with dynamical friction, the center of mass of the stars for the present run show distinct orbital motion around the center of halo mass (Figure 12a). The halo’s center of mass moved less than a grid cell width during any fifty timesteps, during which the star’s center of mass moved up to three cell widths (Figure 12b). This is important in our justifying shortly the value of examining runs with fixed halos.

Run 9 is the high angular momentum version of Run 8. In all other respects the initial conditions of the two runs are the same. The qualitative evolution of the gas is similar in both, although the concentration of gas in the center of the system is lower in the higher angular momentum case. As a result, the halo in Run 9 remains axisymmetric over a larger radius. The initial perturbation on the stars due to the halo is lower in this run than in Run 8, because the stars are not plunging toward the center of the halo’s mass distribution. The stars develop transient arms, but the bar is much less concentrated than in Run 8. Indeed, the central region of the stars remains axisymmetric (Figure 13b). The higher angular

momentum of the stars gives the halo more time to move during each timestep. The stellar center of mass shows a more circular orbit around the halo center of mass than in Run 8 (Figure 14). This is consistent with the decreased perturbation caused by the stars on the halo.

The orbital motion of the stellar component’s center of mass around the halo seen in the last two runs and the associated structure in the star component suggest that such sloshing will have observable effects on galaxies. This belief is strengthened when we compare these results to a “traditional” run, in which the centers of mass of the disk and halo are initially the same and remain the same throughout the run. Labeled Run 10 in Table 3, the non-offset Sc disk shows the typical evolution seen in N -body simulations of the disk. It goes through an initial high- m (multiarmed) spiral phase, and then into a distribution with a persistent bar, without spiral arms (Figure 15). This bar’s long axis extends one quarter of the diameter of the disk.

Run 10 shows profound differences in mass distribution compared to Run 8, which also develops a bar. While the non-offset star distribution maintains an overall disk-shaped structure, virtually all the star particles in Run 8 are either in the bar or in the two weak spiral arms, while there are many stars in an axisymmetric distribution surround the bar throughout Run 10. Furthermore, the bar in Run 8 is much thicker than the bar in Run 10. Although both runs have bars, clearly, the stars in the run with the dynamic halo (Run 8) have followed a different dynamical evolution than the run with the static halo.

The underlying spiral structure created in the halo of these runs is of concern, as there is no observational evidence yet for such structure. To eliminate any nonaxisymmetric effects from a halo, we have made one final set of runs in which the halo remains fixed and axisymmetric. This construct will affect the timescales for the motion of the stellar center of mass around the halo center of mass. However, as noted above, the relatively small

motions of the halo in the low angular momentum situation suggest that this effect will be relatively small for these runs. Indeed, since the halos are expected to be even higher than the 75% of the total galactic mass we have used here, the effect of halo motion will be even less than Runs 8 and 9 indicate. Furthermore, the savings in computer time enabled us to make many more runs with fixed halos than we could have otherwise accomplished.

Runs 11 through 16, 18, and 20 (see Table 3) have displaced stellar centers of mass in fixed halo mass distributions. (Runs 10, 17, and 19 are undisplaced reference runs.) As seen in Table 3, the four parameters we studied can be summarized as follows:

- Initial Offset (Column 2): The initial offset of the disk’s center of mass is either $2\sqrt{2}$ cells (hereafter, “small offset”) or $10\sqrt{2}$ cells (“large offset”) from the halo’s (fixed) center of mass. The small offset runs correspond to 3% of the disk’s radius. A grid cell corresponds to roughly 104 pc.
- Angular Momentum (Column 3): The disk’s center of mass initially has either a low angular momentum or a high angular momentum around the halo center of mass. The high angular momentum runs’ angular momenta are 6% higher than the low angular momentum runs.
- Mass Distribution (Column 4): The halo has a variety of radial mass distributions, as described above. The disk is always an Sc distribution.
- Counter-rotating Component (Column 5): In some of the runs we have set 50% of the star particles in counter-rotating motion.

3.2. Sc Halo Mass Distribution

Run 11 is a small offset, low center of mass angular momentum run. This angular momentum is in the same direction as the stellar angular momentum. As with all the off-center runs reported in this paper, this run shows an initial transient containing more spiral structure than the traditional run (Run 10). In this offset run, the transient is followed by a period of spiral structure with eight or nine arms that combine and decrease in number. This is followed by the establishment of a bar. The bar becomes robust and permanent after 4 rotation periods. The amounts of $m = 1$ (one-armed spiral), and $m = 2$ (bar) motion are comparable to the traditional run. This evolution is summarized in Figures 16 and 17. The center of mass motion of this system spirals around the halo center of mass (Figure 18), as also seen in Levine & Sparke (1998).

Run 12 has an initial offset 5 times larger than Run 11, but is otherwise the same. There is a marked transient one-armed feature that dominates the structure for about $\frac{3}{4}$ of a rotation period. This is followed by several rotation periods in which multiple, flocculent arms spiral out from the $m=1$ arm. The $m=1$ feature persists for the entire run, long after the higher- m structure has dissipated. By the end of 10 rotation periods, there is still no sign of a bar. The center of mass of the disk in this run spirals inward less than is seen in Run 11 (Figure 19).

Run 13 is a high angular momentum version of Run 12. The initial one-armed spiral is 50% stronger than in Run 12. Particularly notable about this run is the formation of several very high density concentrations of N –body particles (Figure 20). These regions persist for about $1\frac{1}{2}$ rotation periods. The end state of the run after 10 rotation periods is qualitatively the same as in Run 12. No bar develops during this run.

The center of mass of Run 13 again spirals in toward the center of the halo mass, but the higher angular momentum of this system results in a longer time during which the

two centers of mass are different. The results of this run are consistent with a similar run presented by Levine & Sparke (1998).

Run 14 is the same as Run 13 except that the initial angular momentum of the disk's center of mass is in the opposite sense to the particles' orbital motion. The dynamics of the resulting one-armed spiral are significantly different than in Run 13. In the present run, the spiral is stationary in angular location for nearly 1.5 rotation periods, while continually expanding radially (Figures 21a, 21b, and 21c). The arm then transforms into a wide, diffuse, leading arm spiral that persists for the remainder of the run. No bar develops during this run.

Recalling the leading arm spirals we saw develop in runs with counter-rotating disks (Comins et al. 1997), we made two Sc runs with counter-rotating disk particles. Both of these runs had low angular momentum orbits for the disk's center of mass.

Run 15 has equal numbers of particles rotating in opposite directions, but is otherwise the same as Run 11. Each of the two counter-rotating sets of particles were separately given the same low angular momentum, in opposite directions. As a result, of course, the total angular momentum of the system was zero. The initial offset served as a perturbation that created tightly wound spirals in the inner region of the disk (Figure 22a). These evolved after $1\frac{1}{2}$ rotation periods into the same single-armed spiral that we saw in Comins et al. (1997). This spiral expanded radially (Figure 22b) as far out as the inner Lindblad resonance where its outer edge bifurcated into spirals like the tongue of a snake (Figure 22c). At this point the spiral arm is about to change directions. While damping thereafter, the spiral structure persisted for the remainder of the run. The center of mass of the entire disk followed a damped oscillation across the halo center of mass throughout the run.

Run 16 also had half of its particles counter-rotating, but otherwise is the same as Run 12. The center of mass of its disk is displaced 5 times farther from the halo center of mass

than in Run 15. Again, the center of mass of the entire disk followed a damped oscillation across the halo center of mass, while the individual counter-rotating halves of the disk separately spiraled inward.

The combined motion created by the initial center of mass offset and the counter-rotating disks led to significantly different behavior than any other run. Within one quarter of a rotation period, the system had developed a reflection-symmetric pattern (Figure 23). After three more rotation periods, a small central bar formed, surrounded by a ring, from which a single, tightly-wound arm spiraled. Thereafter, the bar oscillated in and out of existence, due to energy transfer from the bar to the spiral or ring structure. The spiral arm decayed over 6 rotation periods, reversing its direction several times as it decayed.

3.3. Isothermal Halo Mass Distribution

In order to learn how robust these results are, we then made a series of runs using different halo mass distributions, while keeping the Sc particle disk. In this section we present the runs using an isothermal halo.

Run 17 is a reference case without initial offset. Comparing the results for this case to the comparable Sc case (Run 10), we note that Run 17 develops a bar more quickly, but that this bar is less elliptical than the one in Run 10, extending only over 15% of the disk’s diameter. This bar persists for the entire run. The spiral structure in the two runs (Run 10 and Run 17) are similar in numbers of arms and evolution. While specific differences between the particle dynamics are perceptible between the two runs, they are subjectively very similar throughout.

Run 18 has a high offset disk and low angular momentum. This isothermal run is analogous to Run 12, above. The global spiral features of these two runs are essentially the

same. After the transient spiral stage, however, Run 18 develops a short bar, unlike Run 12. The bar extends over 15% of the disk’s diameter by the fifth rotation period, despite the fact that its Q is by then over 4.0, and climbing. The bar’s $m=2$ Fourier amplitude is 20% less than that of the bar in Run 17.

3.4. Isothermal Halo Mass Distribution With Galactic Black Hole

Run 19 adds the gravitational influence of a supermassive black hole at the halo’s center of mass to Run 17. The black hole’s mass is about $4.2 \times 10^8 M_\odot$, which corresponds to 0.5% of the mass of our model galaxy. The disk in this run has no initial offset. The black hole has the effect of suppressing the bar, while allowing virtually the same transient spiral structure to unfold. The run ends with a high particle concentration near the center of the disk, consistent with the added gravitational potential of the black hole.

Run 20 adds a large offset and high angular momentum to Run 19. Run 20 is therefore analogous to Run 13 (Sc disk and halo). The addition of the black hole mass is significant, especially during the first three rotation periods. Specifically, we observe richer concentrations of particles in Run 20 than in any other run (Figure 24). A bar forms in this run. Its end state is very similar to that of Run 18, differing only in the greater central concentration of particles in the run with the black hole.

4. ANALYSIS AND DISCUSSION

4.1. Theory

Lovelace et al. (1999) studied the eccentric dynamics of a disk with an exponential surface density distribution [$\Sigma_d \propto \exp(-r/r_d)$] represented by a large number of rings and

a central mass $M_0 \sim 10^9 M_\odot$ embedded in a passive dark matter halo. The inner part of the disk $r \lesssim 2.5$ kpc was found to be strongly unstable with e –folding time ~ 30 Myr for the conditions considered. Angular momentum of the rings is transferred outward, and to the central mass if it is present. A trailing one-armed spiral wave is formed in the disk. This differs from the prediction of Baldwin, Lynden-Bell, & Sancisi (1980) of a leading one-armed spiral. The outer part of the disk $r \gtrsim r_d$ is stable and in this region the angular momentum is transported by the wave. This instability appears qualitatively similar to that found by Taga & Iye (1998b) for a fluid Kuzmin disk with surface density $\Sigma_d \propto 1/(1+r^2)^{3/2}$ with a point mass at the center where unstable trailing one-armed spiral waves are found. The present findings do not give evidence of instability of the inner part of the disk, but they do indicate that a long-lasting trailing spiral wave is generated in the disk as found by Lovelace et al. (1999) and Taga & Iye (1998b).

4.2. Effects of Dynamic Halos

Particle and hydrodynamic simulations of a galaxy’s halo lead to significantly different histories for the star particles. This is due in large measure to the dynamical friction that occurs between halo and star particles. Any displacement between the particle halo and stellar centers of mass is quickly damped. The hydrodynamic halo does not damp the stellar motion nearly as much, allowing for prolonged sloshing of the stars and concomitant nonaxisymmetric evolution.

All other things being equal, lower temperature (or lower energy) halo mass leads to more halo displacement as the result of perturbation by a passing galaxy or sloshing stars. These simulations do raise the question as to whether nonaxisymmetric perturbations of the visible matter in galaxies is accompanied by similar changes in the distribution of the underlying halo.

4.3. Results of Perturbed Static Halo Simulations

4.3.1. *Effects of Stellar Disk Displacement from the Halo Center of Mass and of Disk Angular Momentum on Bar Formation*

The runs presented here indicate that bar suppression can be caused by energy redistribution due to the transient motion of the disk center of mass moving toward the halo center of mass. In general, a larger offset of the galactic disk from the halo center is more effective in suppressing the formation of a central bar. The exceptions to this rule are the runs including counter-rotating components (Run 15 and Run 16), where in fact the opposite is observed: the smaller offset produces no bar, but the larger offset does. Comins et al. (1997) showed that the presence of undisplaced 50% counter-rotating components is already an effective suppressor of the formation of a central bar.

The initial offset of the stellar disk’s center of mass was modelled as having occurred in one of two ways: for some runs the stellar disk’s center of mass was given nearly zero initial velocity, causing the center of mass to have a very small angular momentum with respect to the halo’s center. Therefore the stellar disk followed a trajectory that leads nearly through the halo center. In other runs the displaced stellar disk’s center of mass was given a small “push” perpendicular to its offset. This caused the disk to follow a spiral orbit around the halo center. Our results indicate that the amount of the initial displacement of the galactic disk has a much stronger influence on the evolution of the model galaxy than the amount of its angular momentum. In fact, Runs 12 and 13 have identical initial parameters, differing only by their initial angular momentum, and they show no qualitative difference in star distribution by the end of the runs after 10 rotation periods.

4.3.2. Effects of Different Halo Potentials

We found little difference in the effect on bar formation from using different halo mass distributions except for the isothermal potential without a central black hole. Here a bar forms for both a small and a large initial offset. This occurred because the potential of the isothermal mass distribution is about 25% lower in the center of the simulation galaxy, compared to the potential of the other mass distributions at the center of the galaxy. This reduced potential at the galaxy’s center is the result of our effort to fit the isothermal potential closely to the Sc potential over the widest possible range outside the center.

In the case of the isothermal potential with a central black hole, the mass of the black hole was chosen such that its gravitational potential combined with the isothermal potential of the halo produces a potential that is fitted closely to the Sc potential over the entire range of the simulation galaxy, including its center. A mass of $4.2 \times 10^8 M_\odot$ for the black hole achieved this.

4.3.3. Effects of Counter-rotating Stars

Comins et al. (1997) showed that the presence of counter-rotating components in the galactic disk can suppress the formation of a central bar. Those runs were performed without any offset of the stellar components, and their results were similar to our Run 15, which had a small offset and exhibited no sign of a bar at any stage of the run. In contrast to this observation, a large offset as in Run 16 produces an alternating sequence of a central bar and an axisymmetric central feature. This is due to the superposition of two motions: the rotation of the bar, and the back and forth motion of the disk’s center of mass as described above. At its greatest length, the bar extends close to the corotation resonance.

T. Z. and N. F. C. wish to thank Sun Microsystems, Inc., and EDS Data Systems for their generous donations of computers on which most of this work was done. The work of R. V. E. L. was supported in part by NSF grant AST 93-20068.

REFERENCES

Athanassoula, E. 1996, Evolution of Bars in Isolated and in Interacting Disk Galaxies, in *Barred Galaxies*, I.A.U. Colloquium 157, A.S.P. Conf. Series, vol. 91, Buta, R., Crocker, D. A., Elmegreen, B. G., eds., p. 309

Athanassoula, E. 1996, The Fate of Barred Galaxies in Interacting and Merging Systems, in *Barred Galaxies and Circumnuclear Activity*, Lecture Notes in Physics, vol. 474, Sandquist, Aa., Lindblatt, P.O., eds., p. 59

Athanassoula, E. 1999, *N*-Body Simulations of Interacting Disc Galaxies, in *Astrophysica Discs – an EC Summer School*, A.S.P. Conf. Ser., vol. 160, Sellwood, A. J., Goodman, J., eds.

Baldwin, J., Lynden-Bell, D., Sancisi, R. 1980, MNRAS, 193, 313

Binney, J., & Tremaine, S. 1987, Galactic Dynamics

Carlberg, R. G., & Freedman, W. L. 1985, ApJ, 298, 486

Comins, N. F., Zeltwanger, T., Lovelace, R. V. E., & Shorey, P. A. 1997, ApJ, 484, L33

Conselice, C. J. 1997, PASP, 109, 1251

Davidge, T. J., Rigaut, F., Doyon, R., Crampton, D. 1997, AJ, 113, 2094

Hernquist, L., & Mihos, J. C. 1995, ApJ, 448, 41

Jog, C. J. 1997, ApJ, 488, 642

Kornreich, David A., Haynes, Martha P., & Lovelace, R. V. E. 1998, AJ, 116, 2154

Lauer, T. R., et al. 1993, AJ, 106, 143

Lauer, T. R., et al. 1996, ApJ, 471, L79

Levine, S. E., & Sparke, L. S. 1998, ApJ, 496, L13

Lotan-Luban, P. 1990, Ph.D. Thesis, Iowa State University

Lovelace, R. V. E., Zhang, L., Kornreich, D. A., & Haynes, M. P. 1999, ApJ, 524, 634

Miller, R. H., & Smith, B. F. 1988, in *Applied Mathematics, Fluid Mechanics, and Astrophysics: A Symposium in Honor of C. C. Lin*. D. J. Benney, F. H. Shu, & C. Yuan, eds. (Singapore: World Scientific)

Miller, R. H., & Smith, B. F. 1992, ApJ, 393, 508

Miwa, T., & Noguchi, M. 1998, ApJ, 499, 149

Noguchi, M. 1996, ApJ, 469, 605

Richter, O., Sancisi, R. 1994, A&A, 290, 9

Rix, H. W., & Zaritsky, D. 1995, ApJ, 447, 82

Schoenmakers, R. H. M., Franx, M., & de Zeeuw, P. T. 1997, MNRAS, 292, 349

Schroeder, M. C. 1989, Ph.D. Thesis, University of Maine

Schroeder, M. C., & Comins, N. F. 1989, ApJ, 346, 108

Sellwood, J. A., 1983, Disk Stability, in *Internal Kinematics and Dynamics of Galaxies*, I.A.U. Symposium, vol. 100, Athanassoula, E., ed., p. 197

Sellwood, J. A., & Carlberg, R. G. 1984, ApJ, 282, 61

Sellwood, J. A., & Merritt, D. 1994, ApJ, 425, 530

Shorey, P. A. 1996, Ph.D. Thesis, University of Maine

Struck, C. 1999, Galaxy Collisions, Physics Reports, vol. 321

Swaters, R. A., Schoenmakers, R. H. M., Sancisi, R., van Albada, T. S. 1999, MNRAS, 292, 349

Syer, D., & Tremaine, S. 1996, MNRAS, 281, 925

Taga, M., & Iye, M. 1998a, MNRAS, 299, 111

Taga, M., & Iye, M. 1998b, MNRAS, 299, 1132

Zaritsky, D., & Rix, H. W. 1997, ApJ, 477, 118

Fig. 1.— Rotation curves for the Sc, isothermal, and isothermal plus black hole potentials. The fraction of mass in the halo was chosen so that the isothermal potential stabilizes against the formation of a bar. An Sc potential with the same total mass fraction and with no initial disk offset does allow a bar to develop. The radius is given in grid cells, where one grid cell corresponds to about 104 pc.

Fig. 2.— The motion of the disk’s center of mass, relative to the motion of the halo’s center of mass, for the cold halo case comprised of N -body components. The motion starts at (0,0,2) when the two components almost coincide at the beginning of the simulation. The disk’s center of mass then “dances” counterclockwise around the halo’s center of mass. The numbers along the path are time units in revolutions.

Fig. 3.— Same as figure 2, but for the hot halo N -body case. The beginning of the motion is again at point (0,0,2). The numbers along the path are time units in revolutions.

Fig. 4.— The center of mass separation between the halo and the stars for the cold gas case. The motion starts at (-0.1,0,1). The numbers along the path are time units in revolutions.

Fig. 5.— Gas distribution for Run 5.

Fig. 6.— Star distribution for Run 5.

Fig. 7.— Karachentsev 64, a pair of interacting galaxies in Andromeda. Photo Credit: NOAO/NSF

Fig. 8.— The center of mass separation between the halo and the stars for the hot gas case with intruder (Run 5).

Fig. 9.— The center of mass separation between the halo and the stars for Run 6. After about 2.5 rotation periods the two centers of mass stay very close together for the remainder of the run, and therefore no further time indicators are included in this plot.

Fig. 10.— The stellar density distribution of Run 7 at three different time steps.

Fig. 11.— Run 8: (a) Hot gas distribution, (b) star distribution.

Fig. 12.— Run 8: (a) The center of mass separation between the halo and the stars. (b) The distances traveled by the centers of mass of the stars and the halo, respectively.

Fig. 13.— Run 9: (a) Hot gas distribution (the image at $t = 6.040$ revolutions is corrupted), (b) star distribution.

Fig. 14.— Run 9: The center of mass separation between the halo and the stars.

Fig. 15.— Run 10: Star distribution.

Fig. 16.— The $m=1$ (one-armed) behavior of 4 Sc runs labeled 10, 11, 12, and 13.

Fig. 17.— The $m = 2$ (bar) behavior of the same four runs used in Figure 16.

Fig. 18.— Center of mass motion of the disk in Run 11. The halo in this run is fixed,

with its center of mass located at (129,129). The numbers along the path are time units in revolutions.

Fig. 19.— Center of mass motion of the disk in Run 12. The halo in this run is fixed, with its center of mass located at (129,129). The numbers along the path are time units in revolutions.

Fig. 20.— Particle mass distribution for Run 13 (Sc mass distribution, large offset, high, corotating angular momentum).

Fig. 21.— Run 14 shows the initial stationary trailing-arm spiral expanding radially and then as a leading arm spiral that persists for the rest of the run. (a) This is at 0.42 rotation periods. (b) At 0.83 rotation periods. (c) At 1.7 rotation periods.

Fig. 22.— Run 15 has equal numbers of particles orbiting in opposite directions and begins with a small offset and low angular momentum. (a) This is at 1.6 rotation periods and shows an initially tight one-armed spiral. (b) At 5.0 rotation periods: The spiral expands. (c) At 6.0 rotation periods: The spiral bifurcates into two spirals.

Fig. 23.— This image from Run 16 (equal numbers of particles orbiting in opposite directions, a large initial offset from the halo potential, and low angular momentum) after 0.25 rotation periods shows the formation of a reflection-symmetric pattern. This run also shows the formation of non-axisymmetric structures.

Fig. 24.— Mass concentrations in Run 20 (isothermal halo, black hole, Sc disk, large offset, high angular momentum). These transient features persist for about 3 rotation periods. Such features are seen in spiral galaxies such as M101.

Table 1. Runs with Intruder, dynamic halo

Run #	Halo	$Q_{0,halo}$	T_0^a	Description
1	N -body, dynamic	0.3		cold, clumpy
2	N -body, dynamic	5.0		hot, clumpy
3	Hydro, dynamic		0.5 K	cold, smooth
4	Hydro, dynamic		5.0 K	cool, smooth
5	Hydro, dynamic		5×10^5 K	hot, smooth

^aMeasured at the half mass radius

Table 2. Dynamic Halo Simulations without Intruder

Run #	Particle Offset ^a	Particle Type	Angular Momentum ^b	Final Bar?
6	$10\sqrt{2}$	N -body	low, CCW	no
7	$10\sqrt{2}$	N -body	high, CCW	no
8	$10\sqrt{2}$	Hydro	low, CCW	yes
9	$10\sqrt{2}$	Hydro	high, CCW	no

^aThis is the initial offset of the star particles from the halo’s center of mass.

^bThe initial particle angular momentum can be either 0, low, or high, and it can be either clockwise (CW) or counterclockwise (CCW).

Table 3. Simulations with a fixed halo

Run #	Particle Offset ^a	Angular Momentum ^b	Mass Distribution ^c	Counter-rotating Component? ^d	Final Bar?
10	0	0	Sc	no	yes
11	$2\sqrt{2}$	low, CCW	Sc	no	yes
12	$10\sqrt{2}$	low, CCW	Sc	no	no
13	$10\sqrt{2}$	high, CCW	Sc	no	no
14	$10\sqrt{2}$	high, CW	Sc	no	no
15	$2\sqrt{2}$	low, CCW	Sc	yes	no
16	$10\sqrt{2}$	low, CCW	Sc	yes	yes
17	0	0	Isothermal	no	yes
18	$10\sqrt{2}$	low, CCW	Isothermal	no	yes ^e
19	0	0	Isothermal plus black hole	no	no
20	$10\sqrt{2}$	high, CCW	Isothermal plus black hole	no	yes ^f

^aThis is the initial offset of the star particles from the halo's center of mass.

^bThe initial particle angular momentum can be either 0, low, or high, and it can be either clockwise (CW) or counterclockwise (CCW).

^cThis is the mass distribution of the static halo. The mass distribution of the star particles was that of an Sc disk in each run.

^dIf counter-rotating components are present, then 50% of the star particles rotate clockwise, and 50% rotate counterclockwise.

^e $m = 2$ (bar) Fourier amplitude 20% lower than in Run 17.

^fSmall bar only.

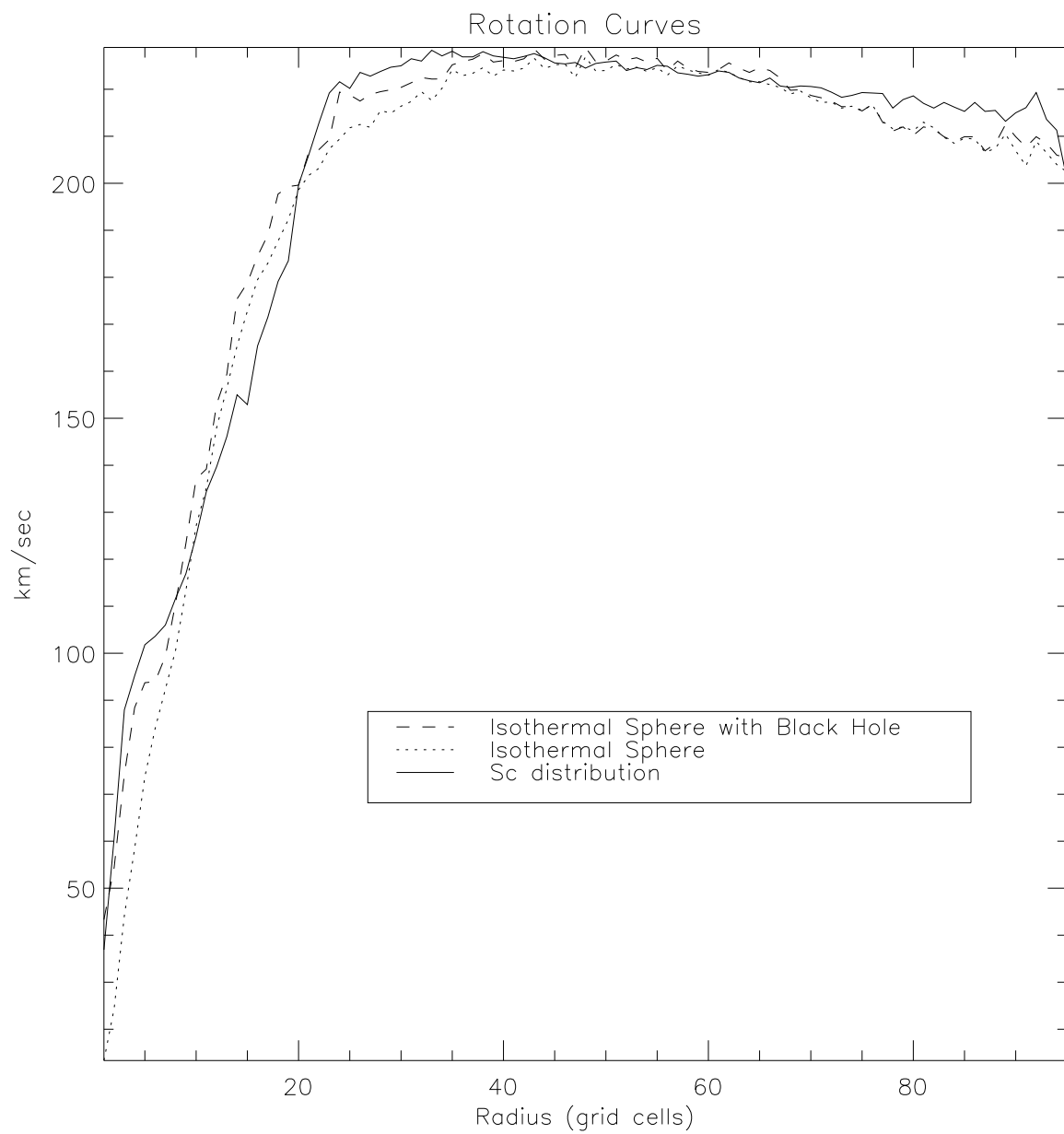


Fig. 1.—

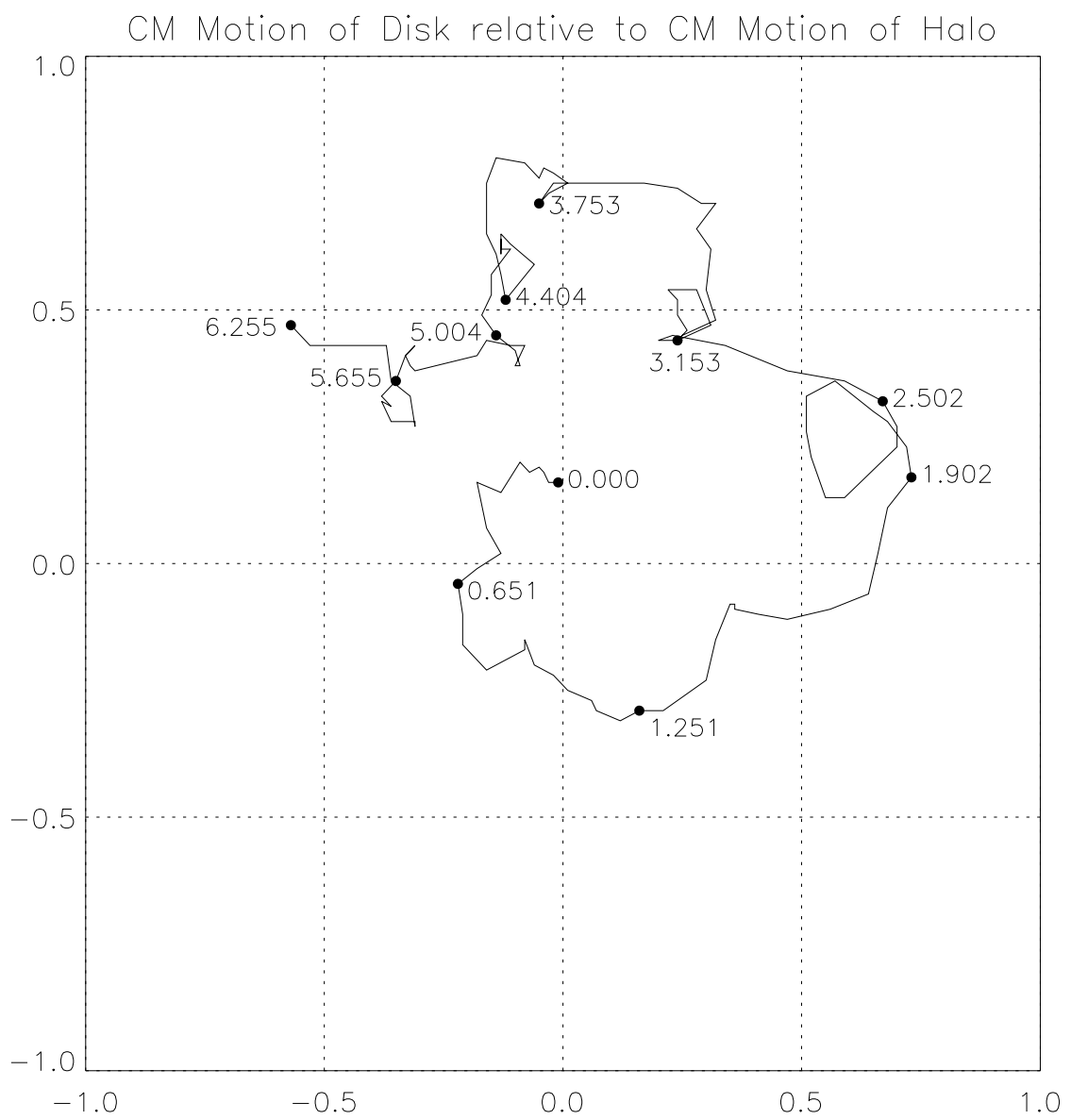


Fig. 2.—

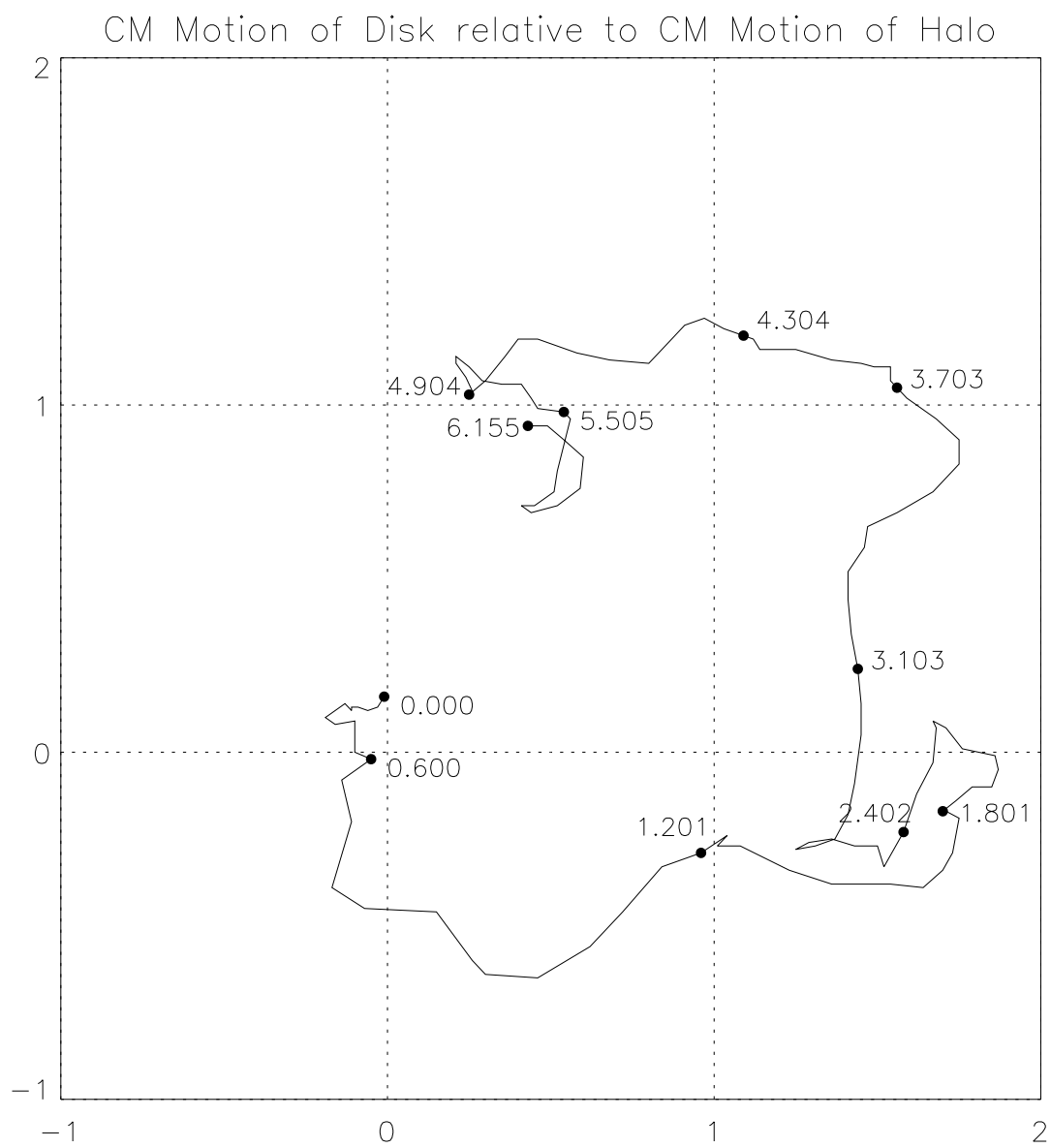


Fig. 3.—

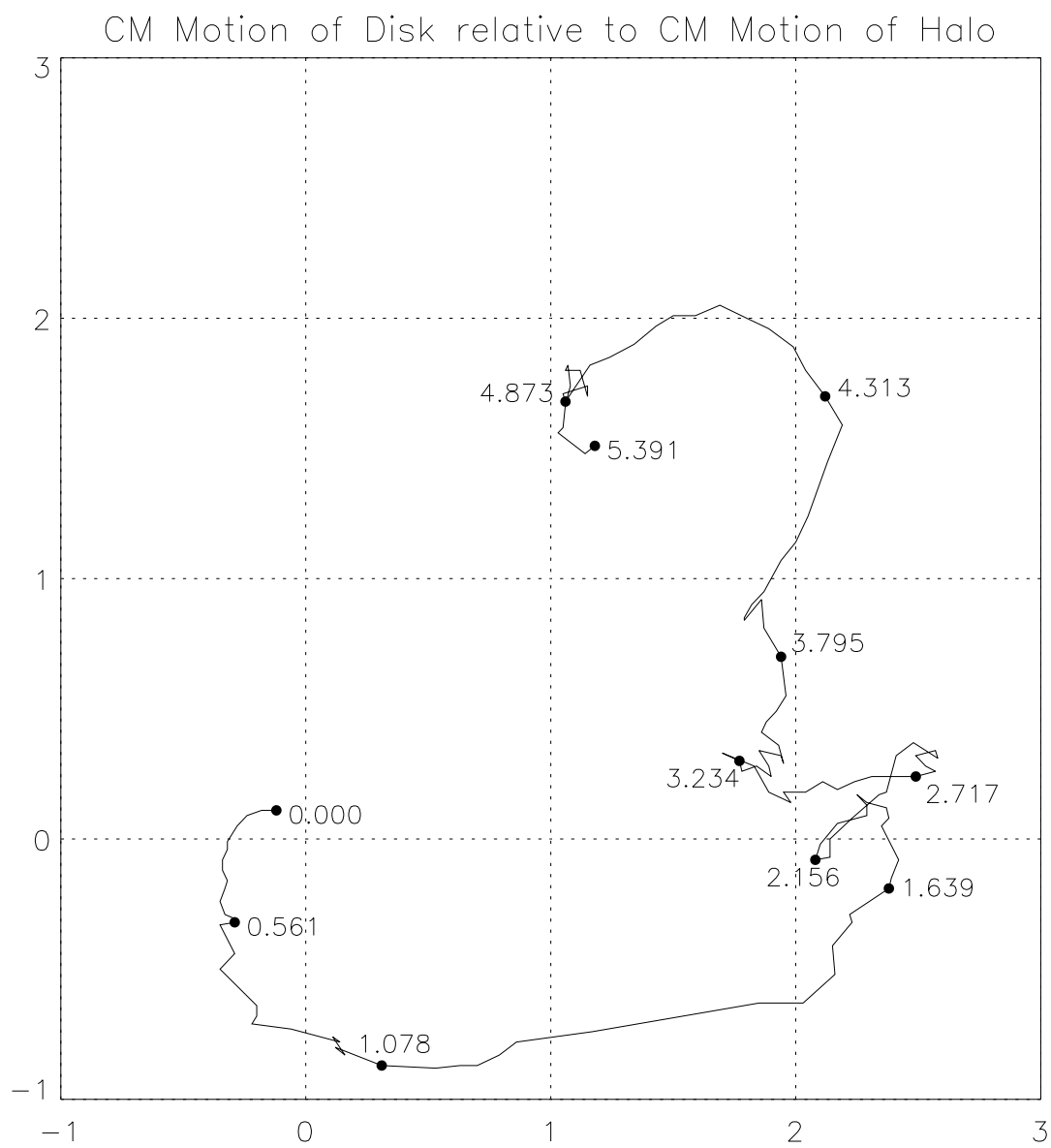


Fig. 4.—

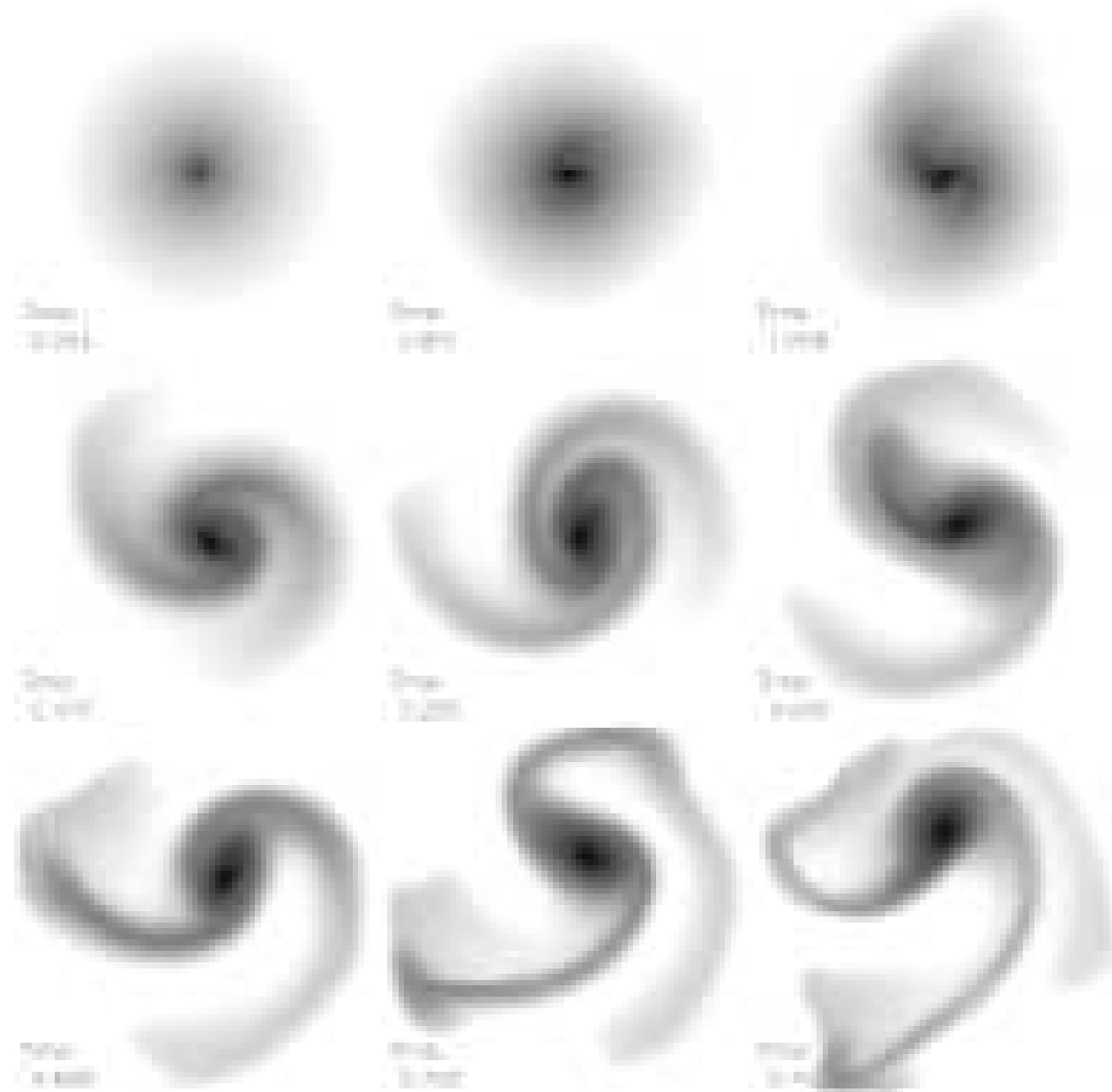


Fig. 5.—

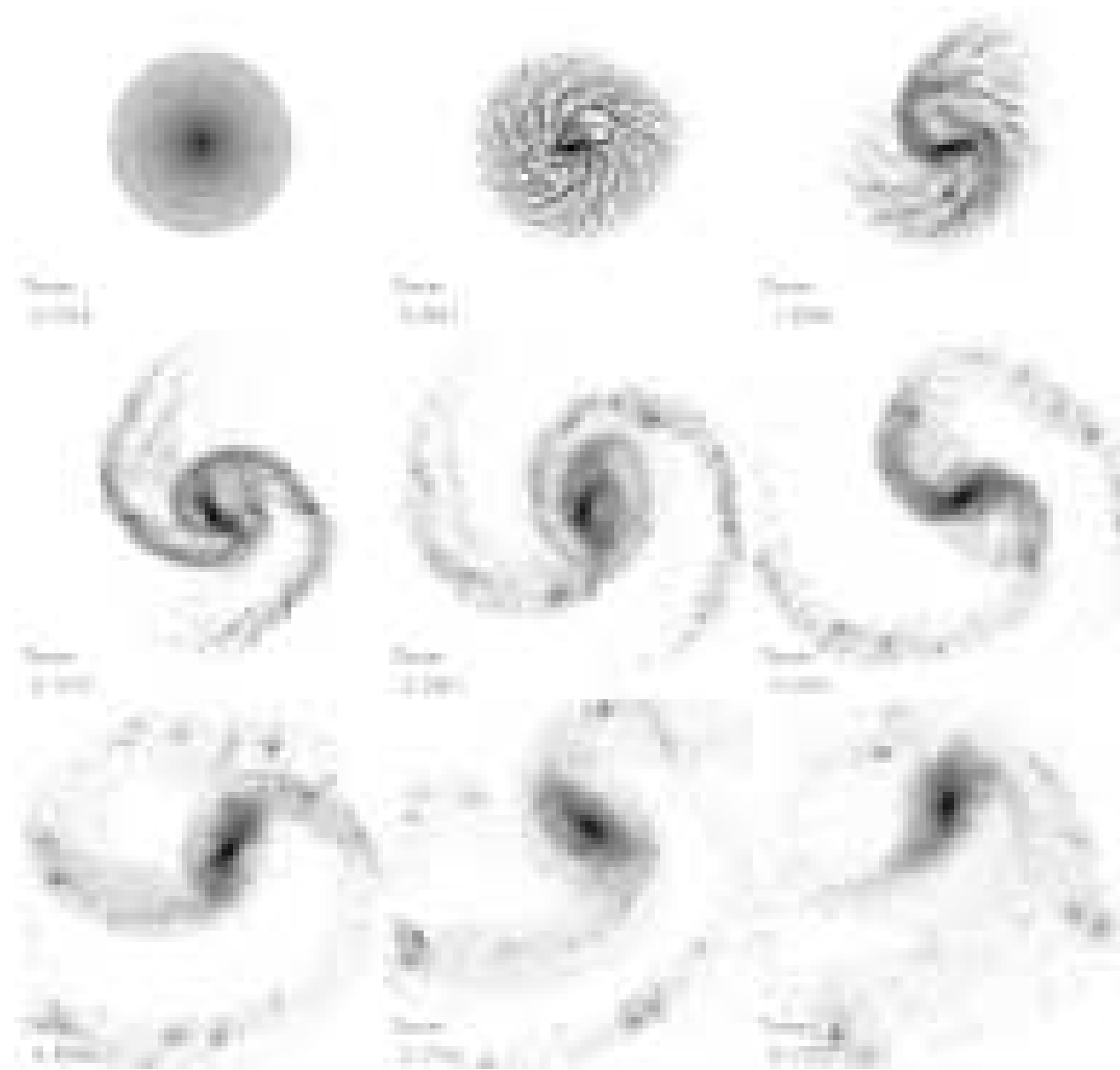


Fig. 6.—

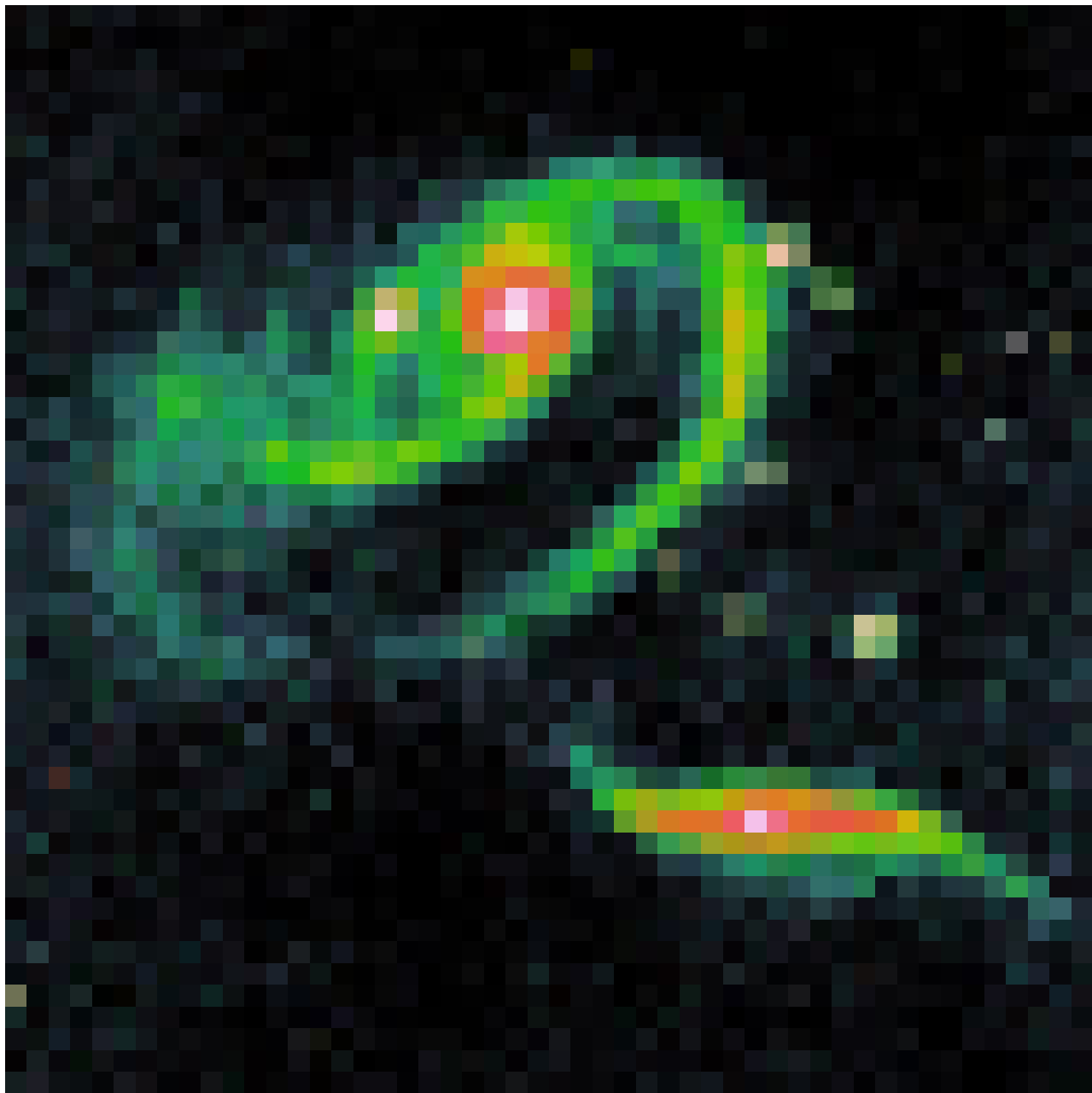


Fig. 7.—

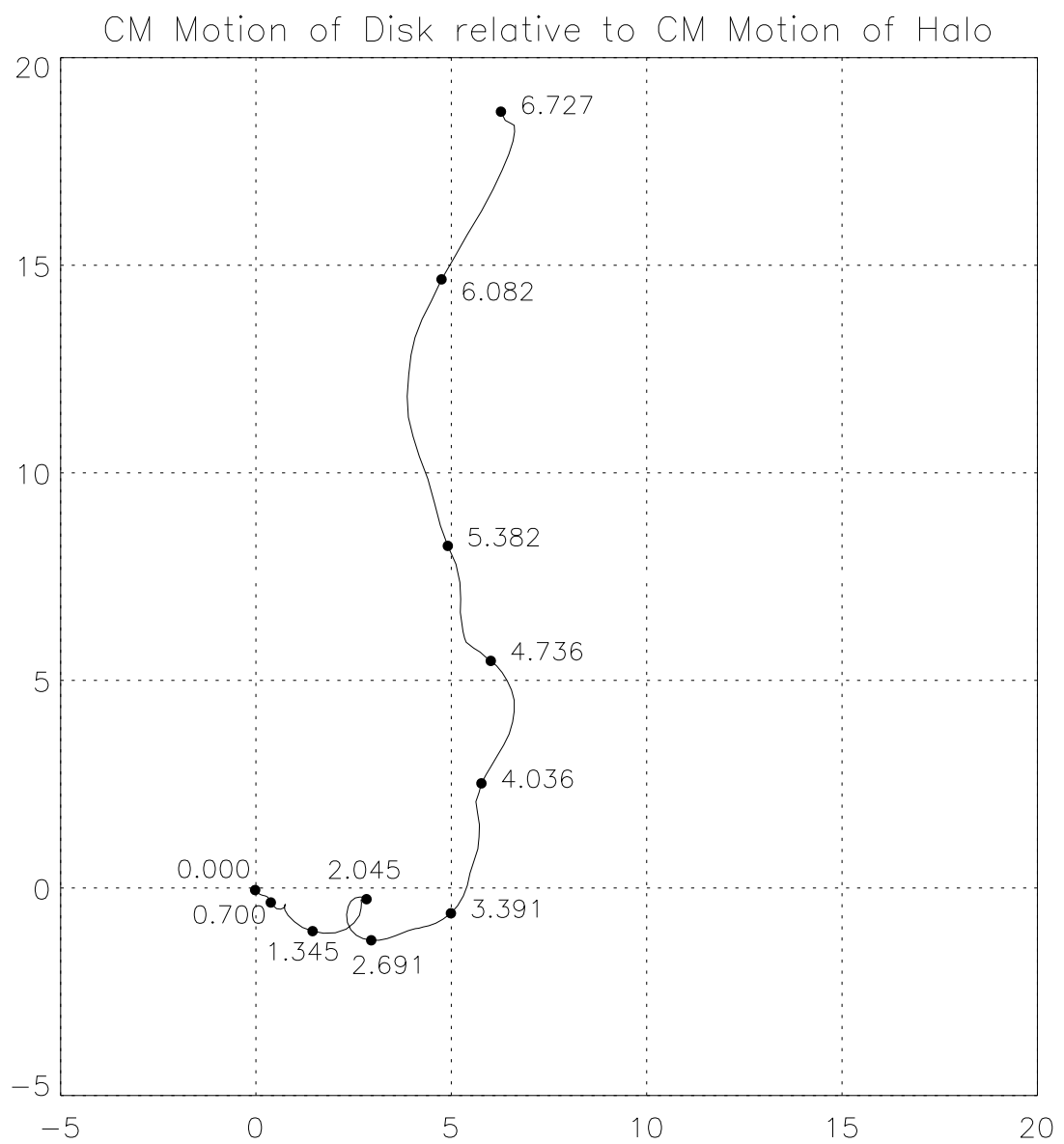


Fig. 8.—

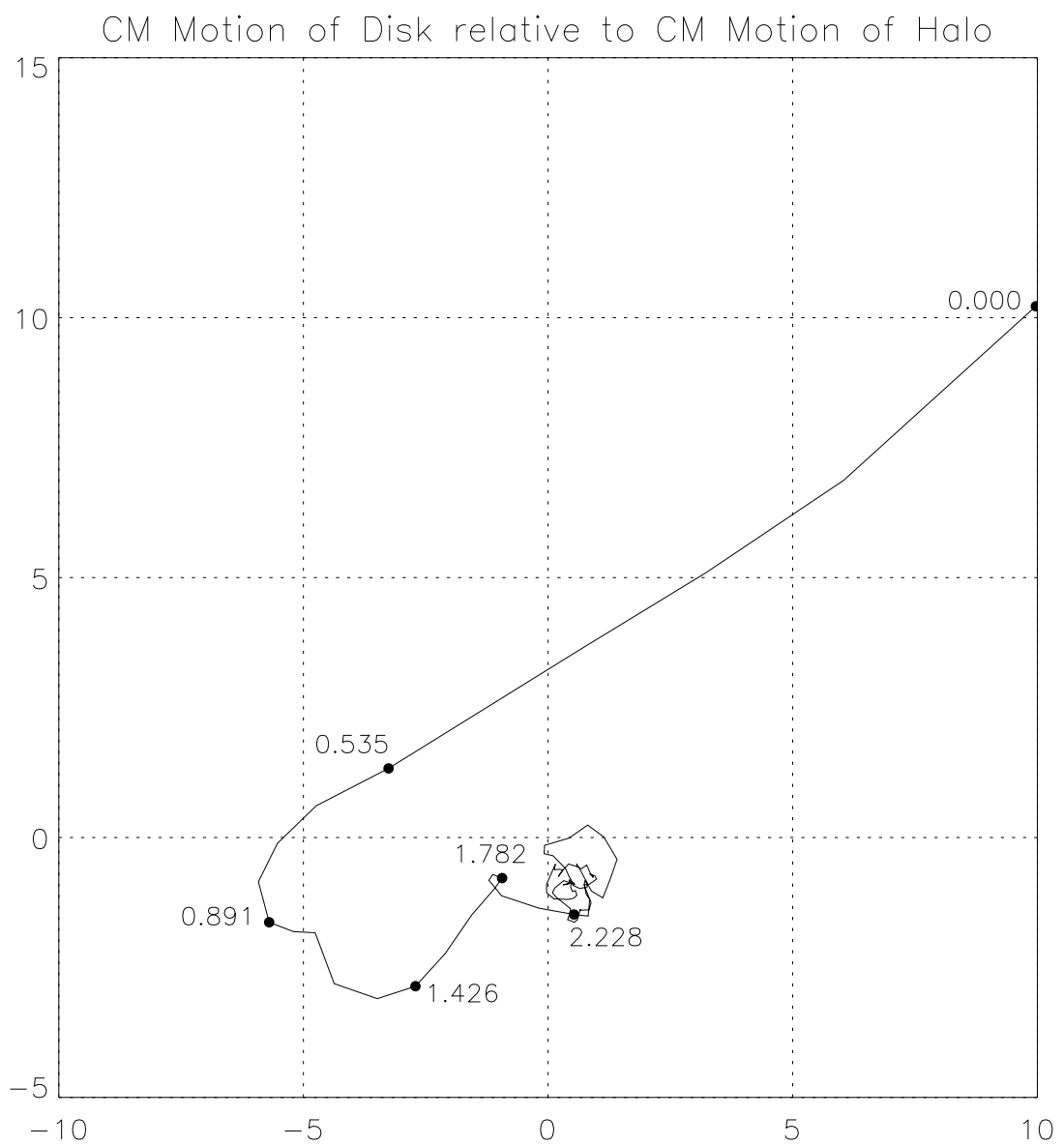


Fig. 9.—

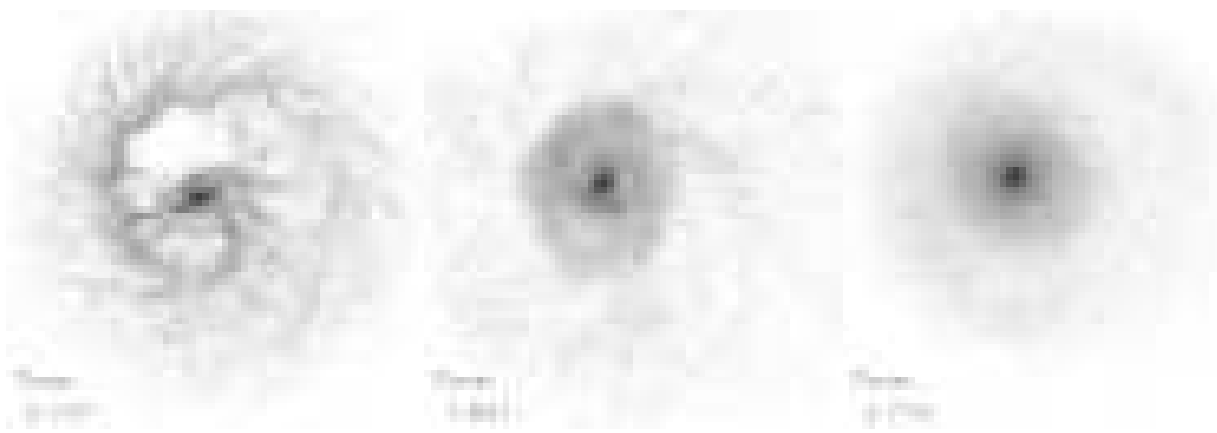


Fig. 10.—

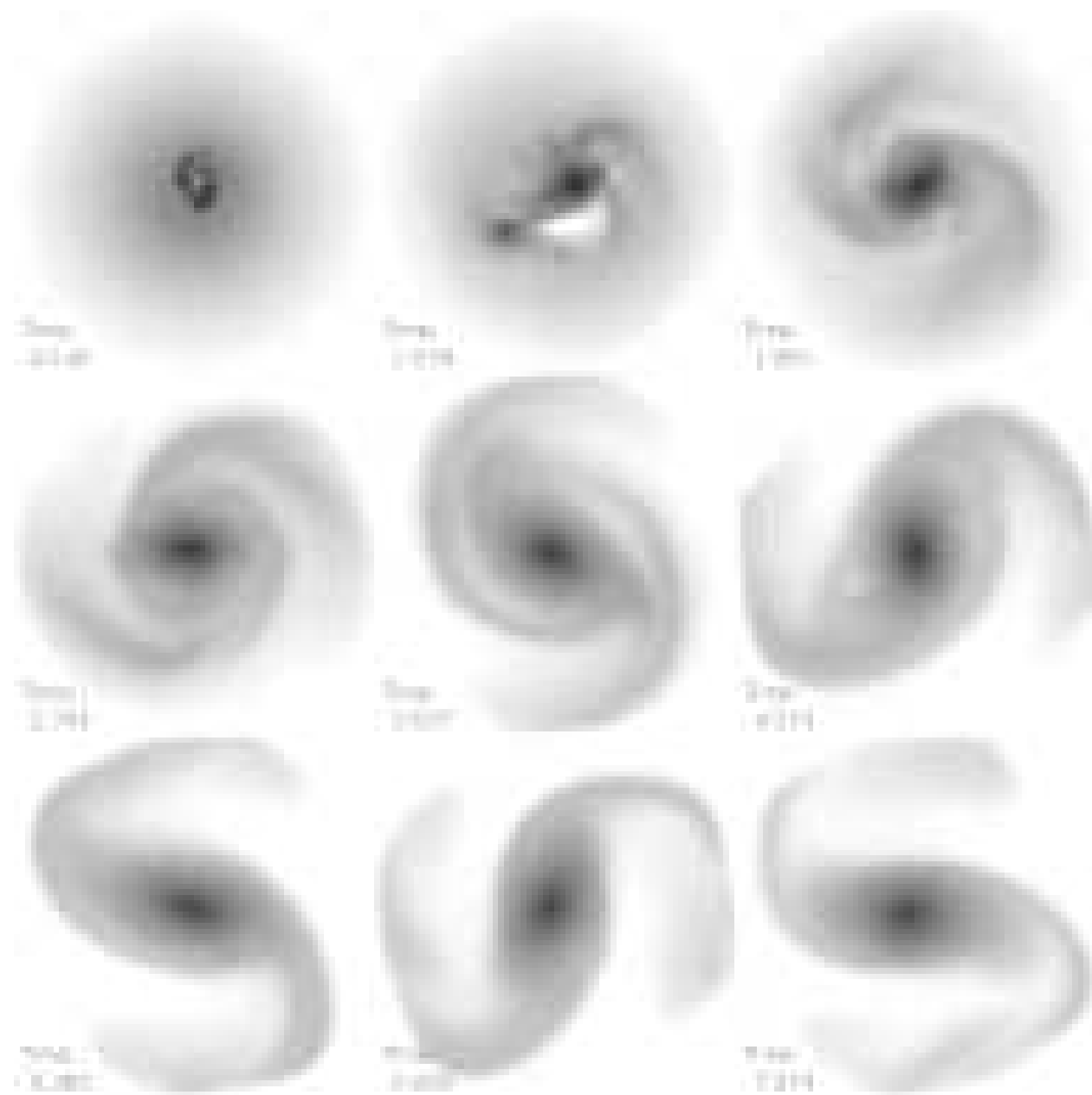


Fig. 11a.—

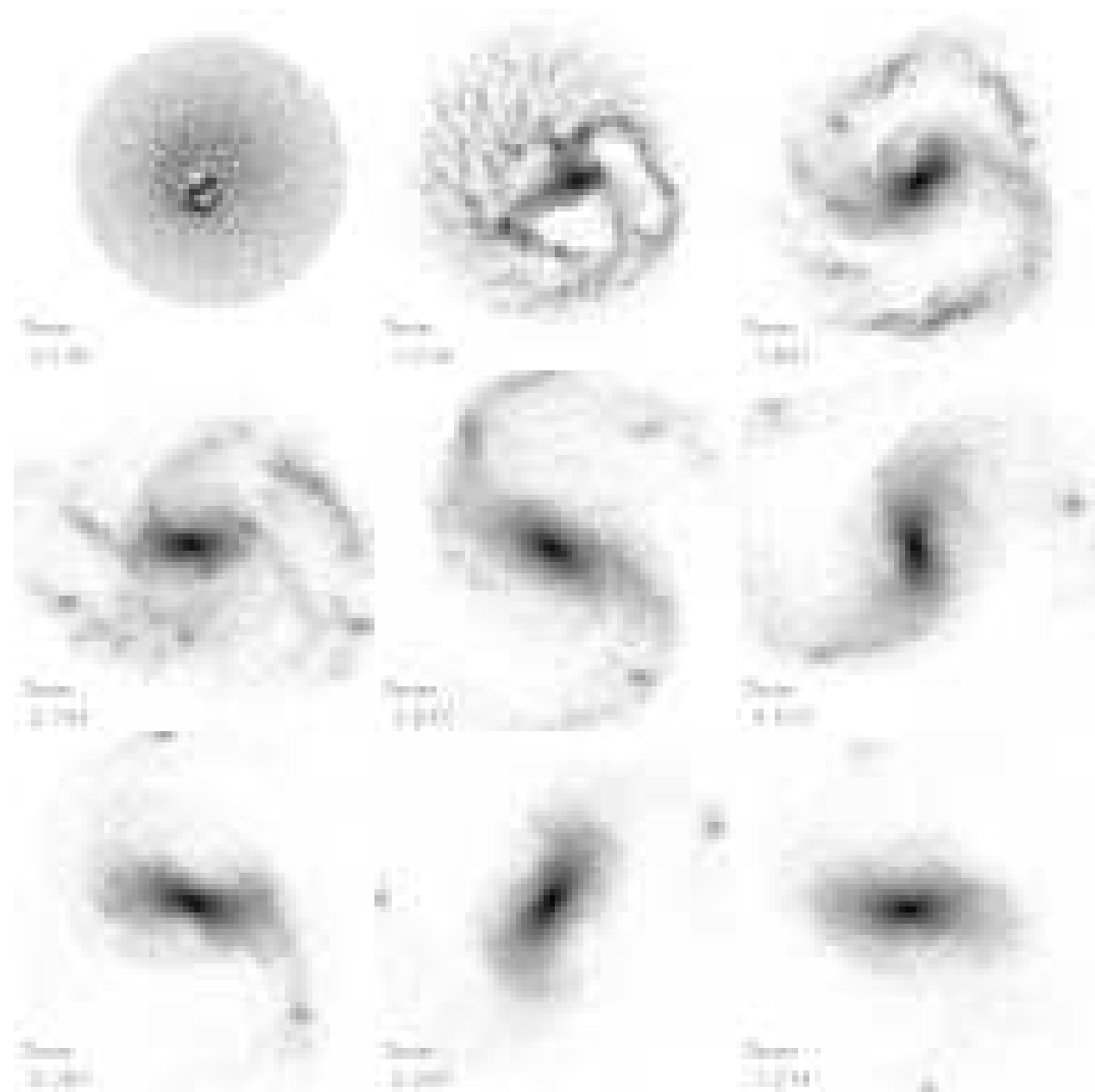


Fig. 11b.—

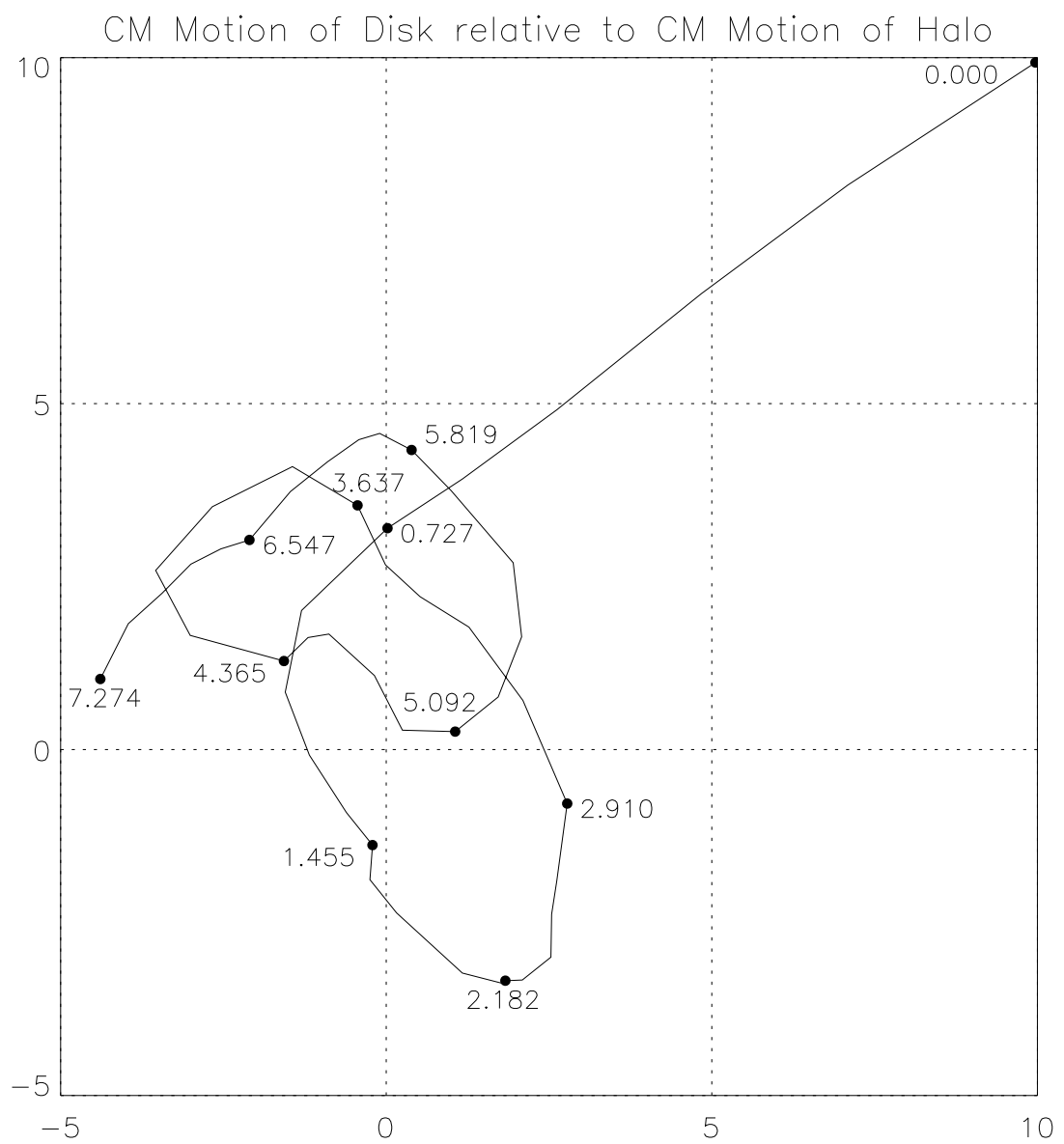


Fig. 12a.—

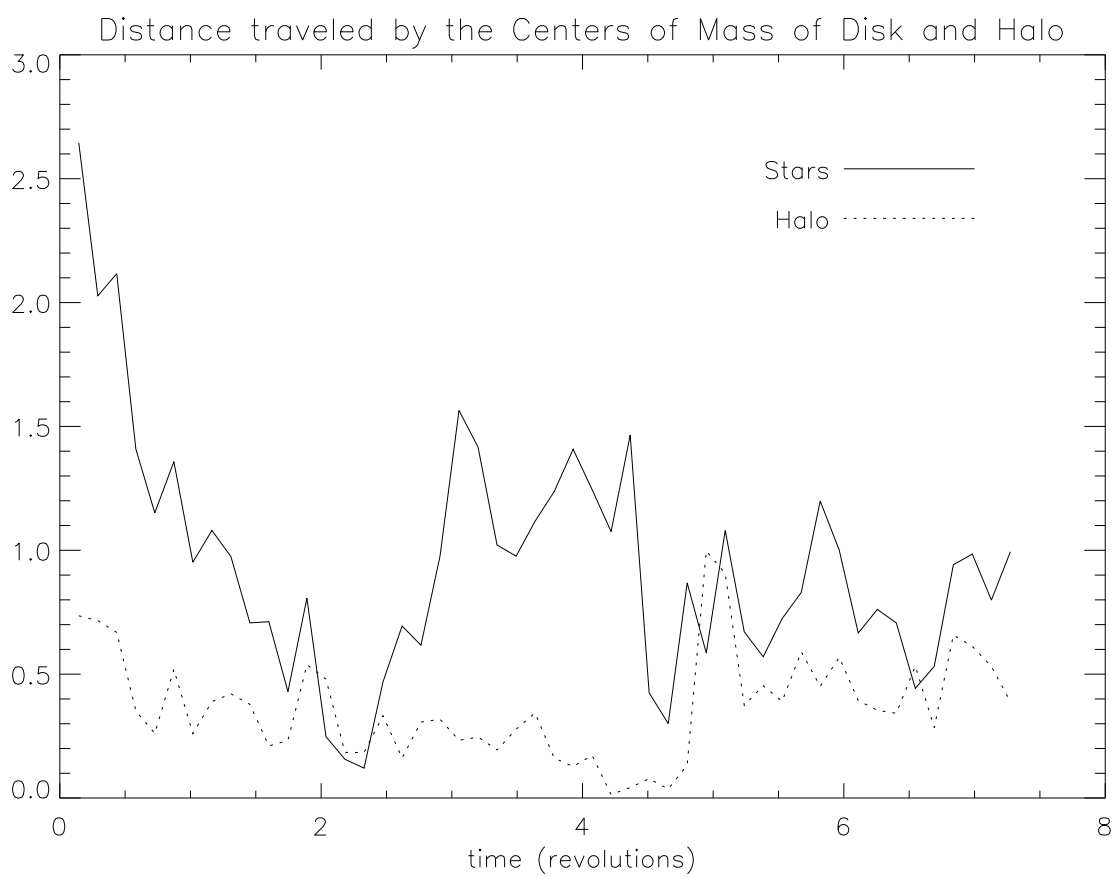


Fig. 12b.—

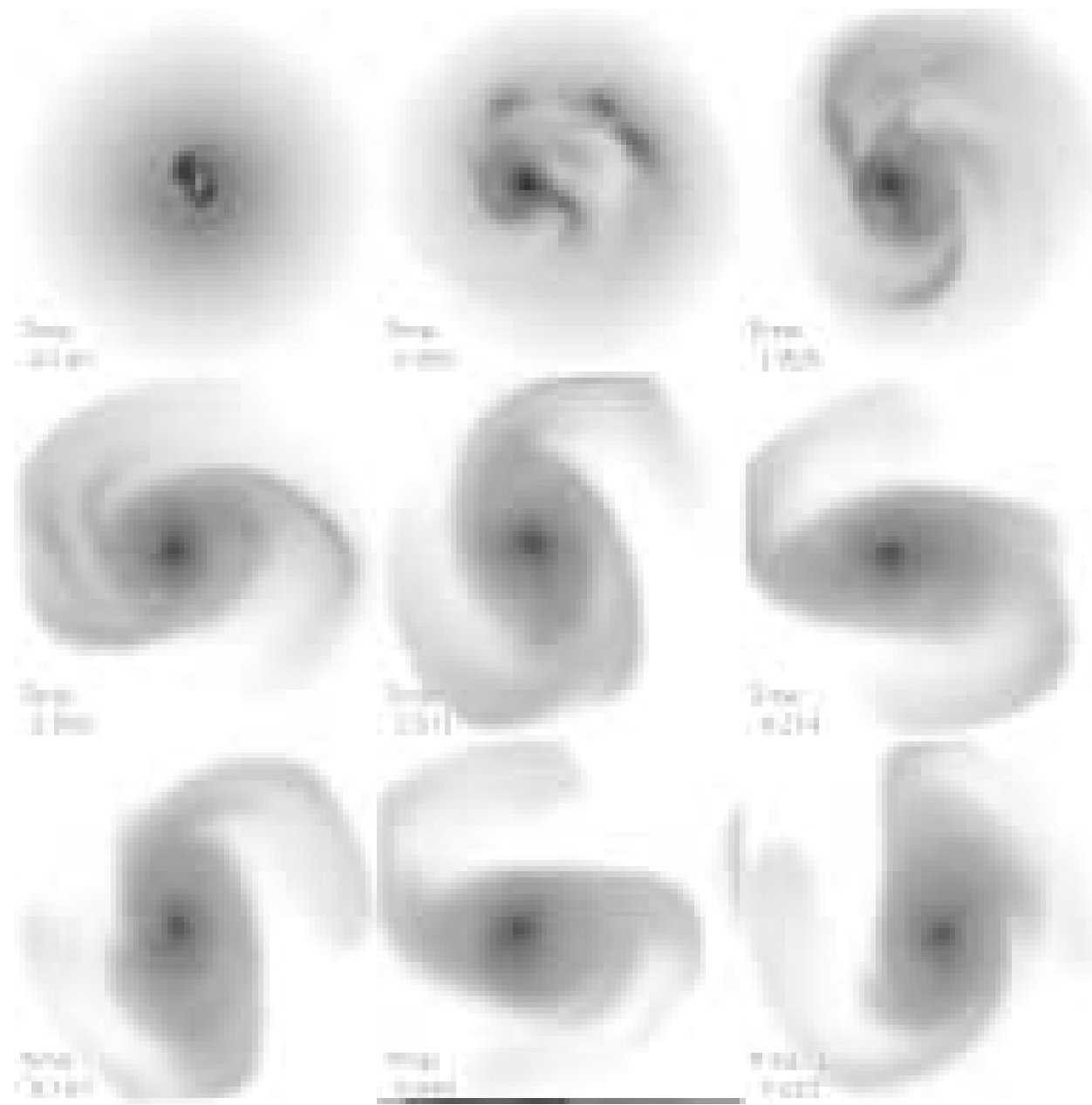


Fig. 13a.—

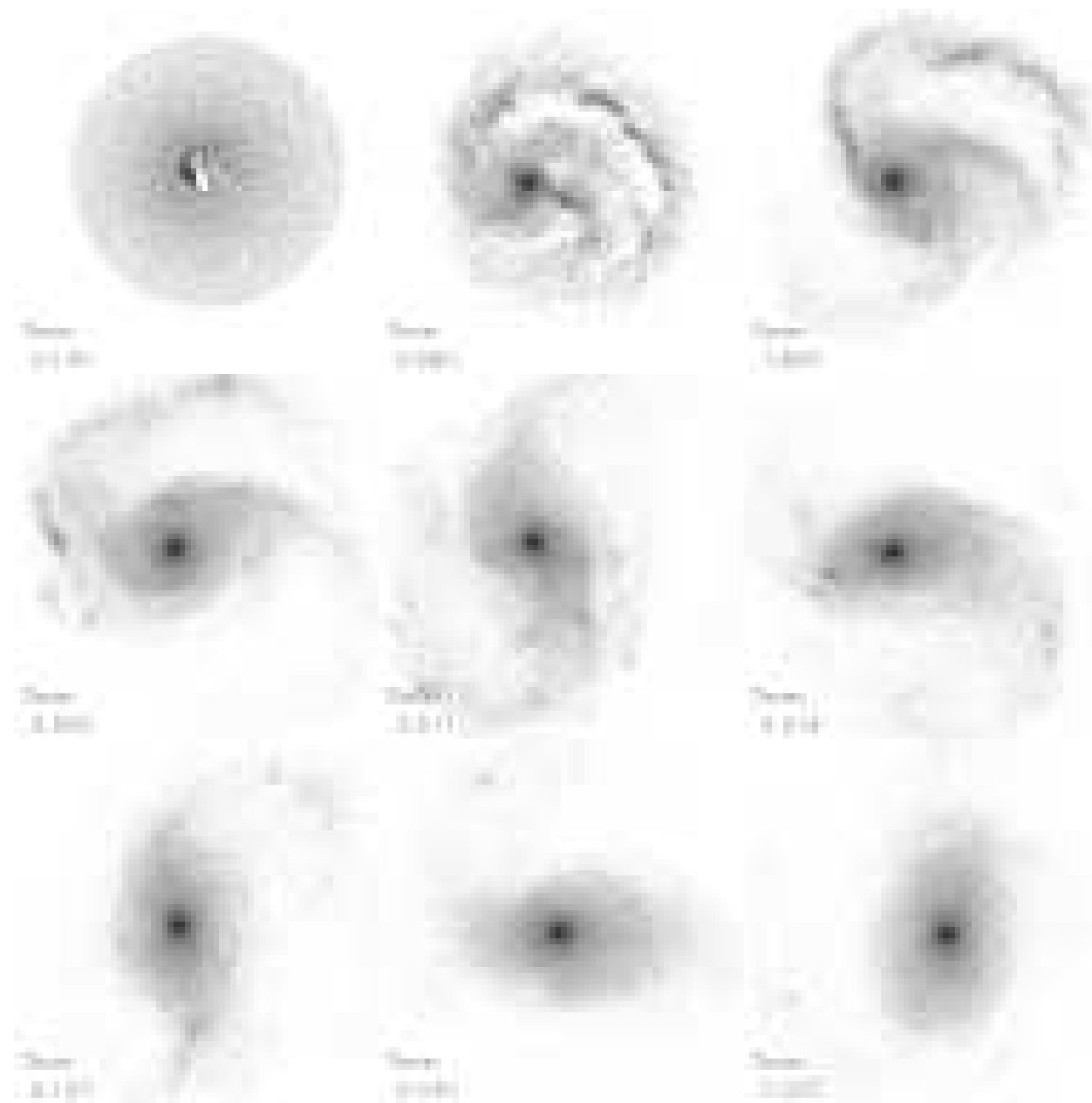


Fig. 13b.—

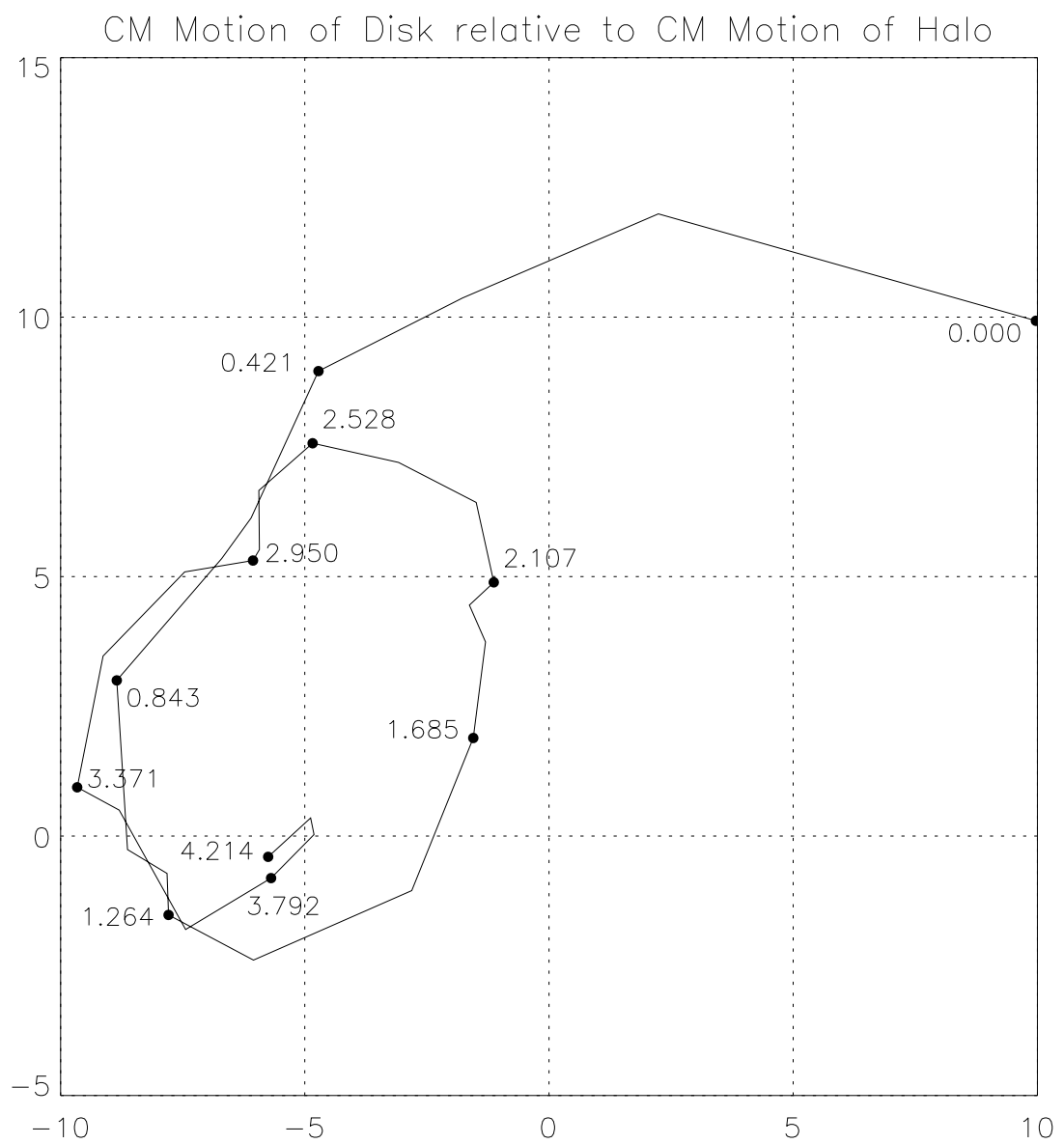


Fig. 14.—

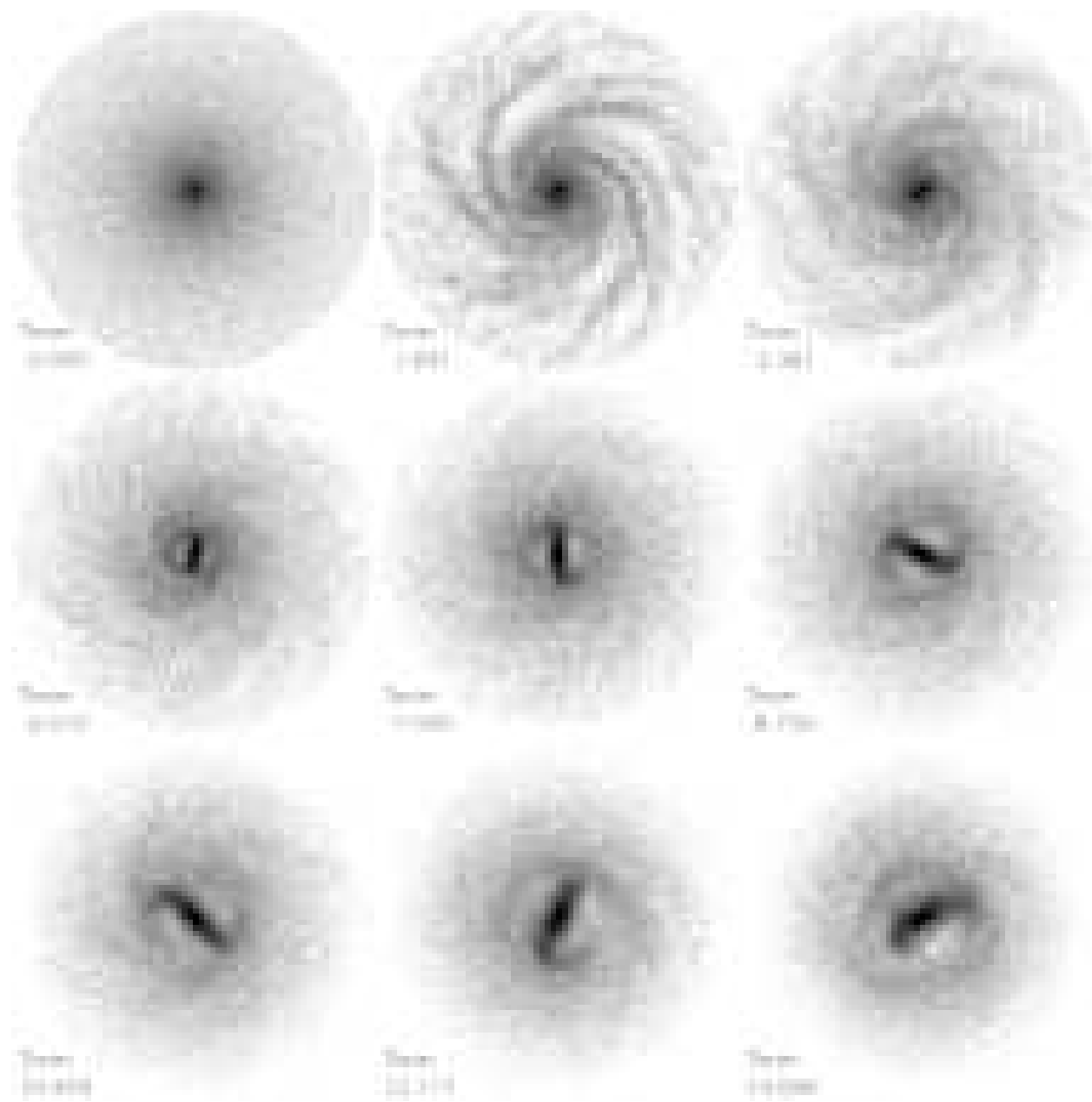


Fig. 15.—

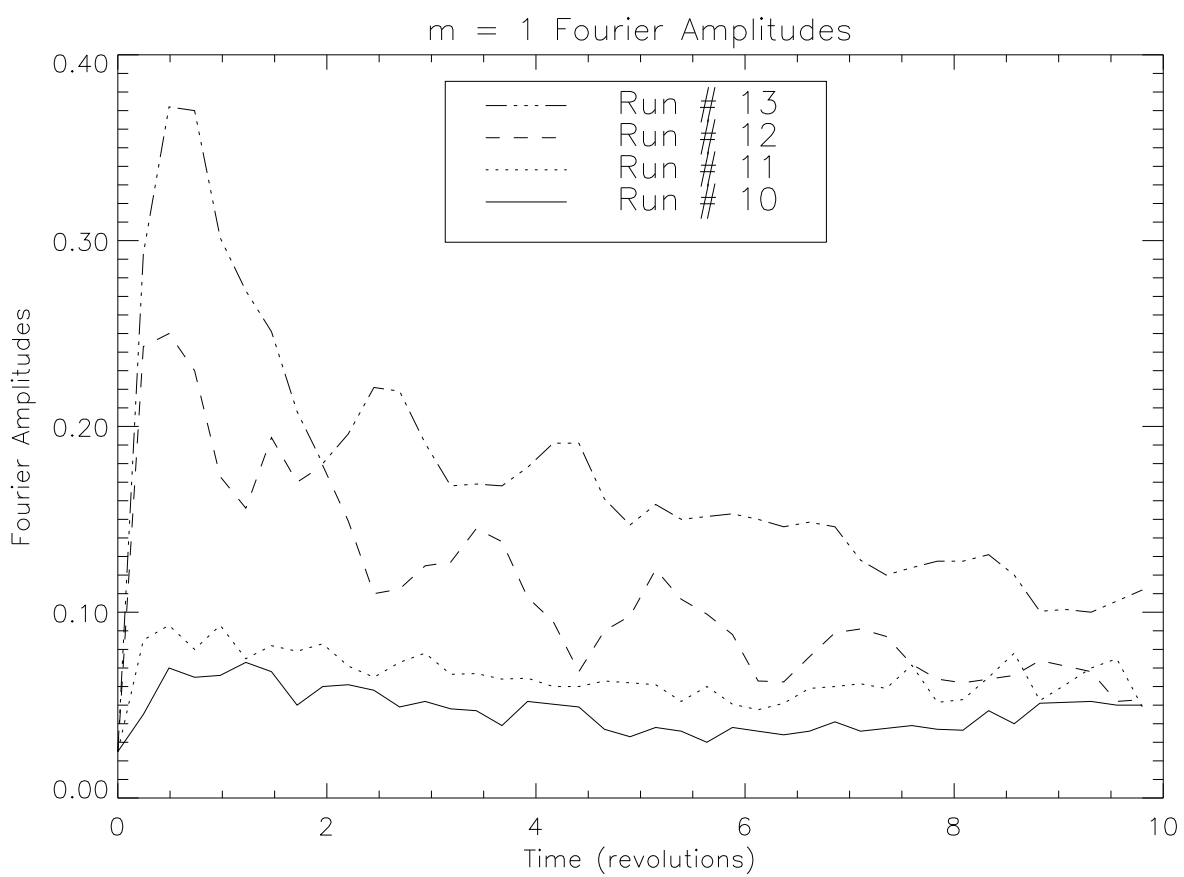


Fig. 16.—

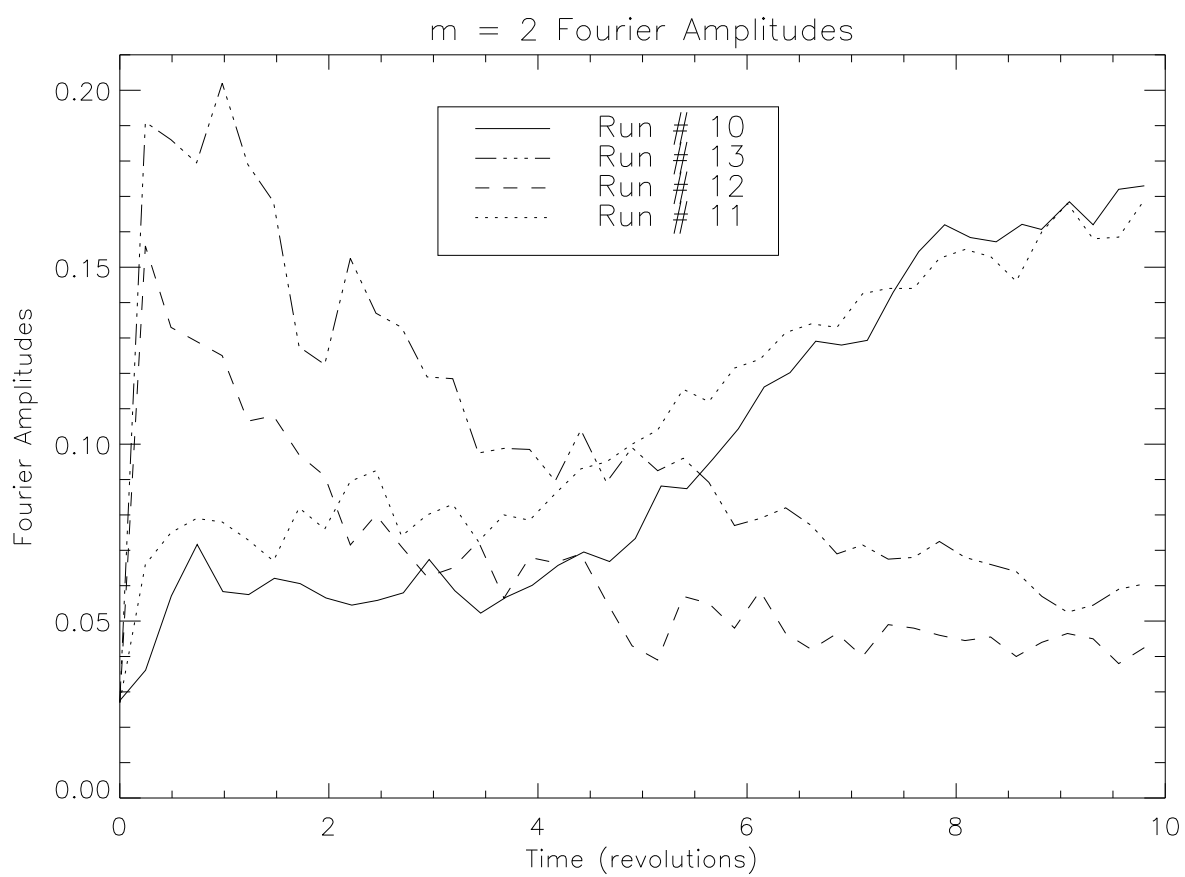


Fig. 17.—

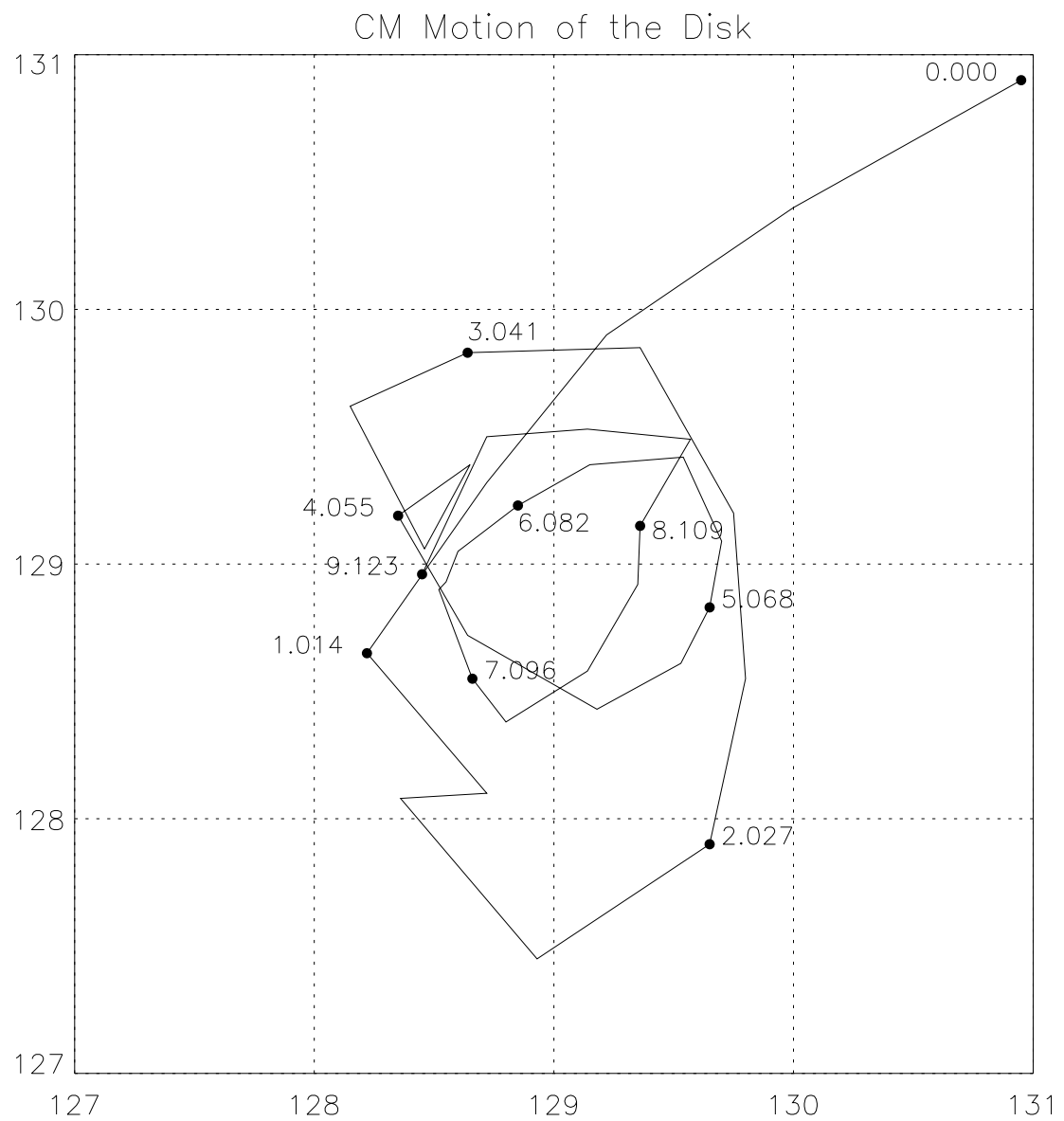


Fig. 18.—

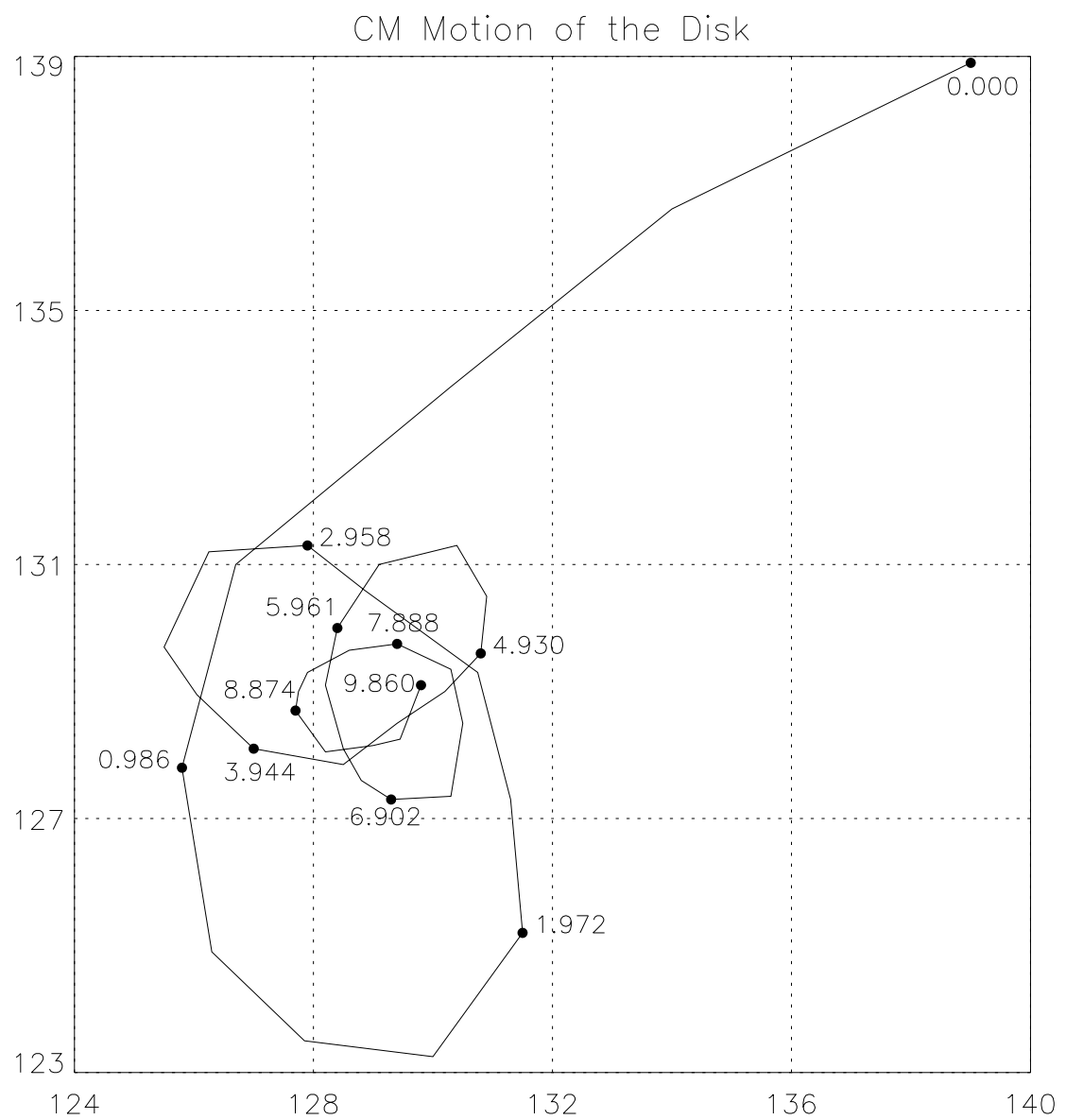


Fig. 19.—

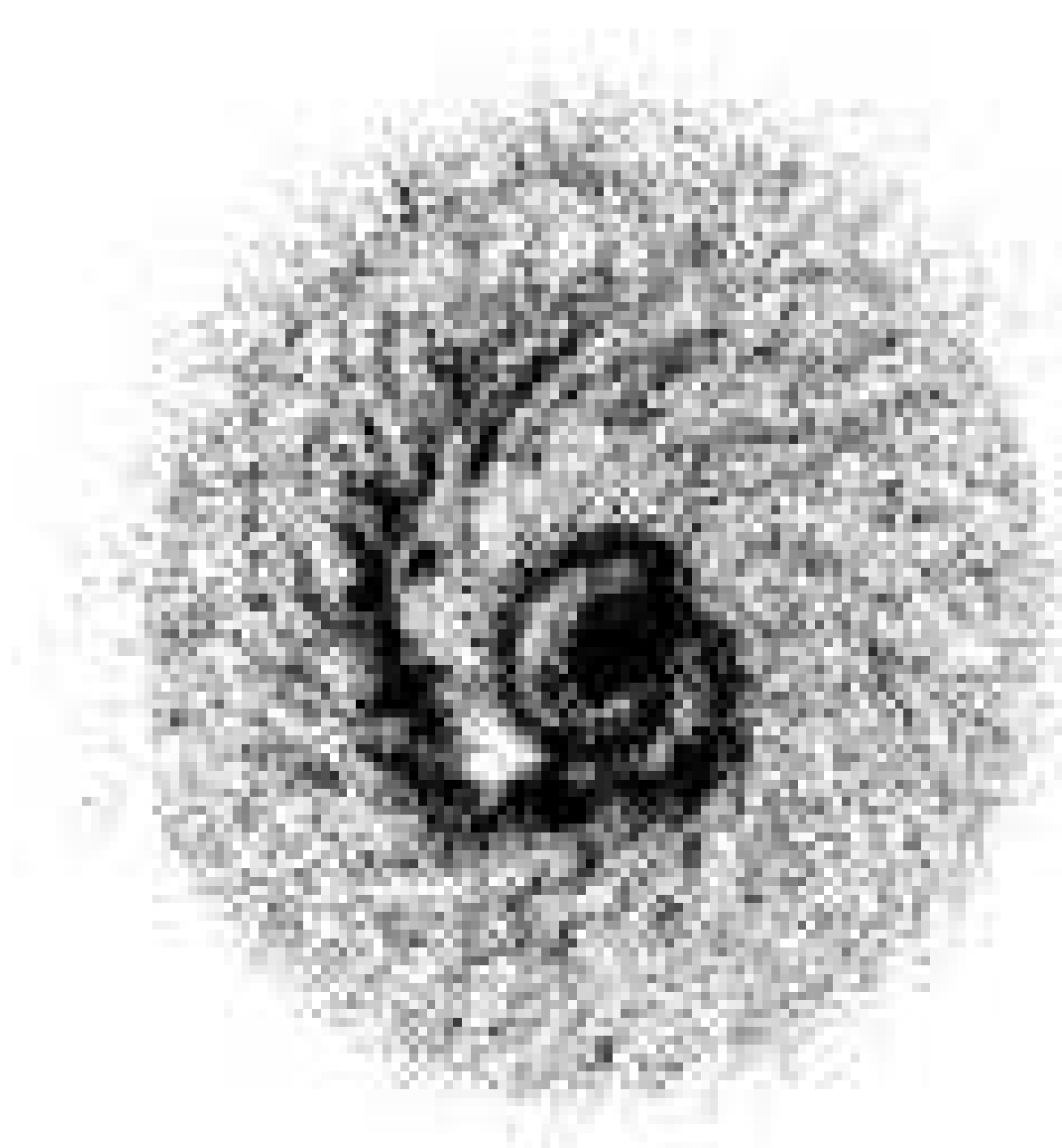


Fig. 20.—

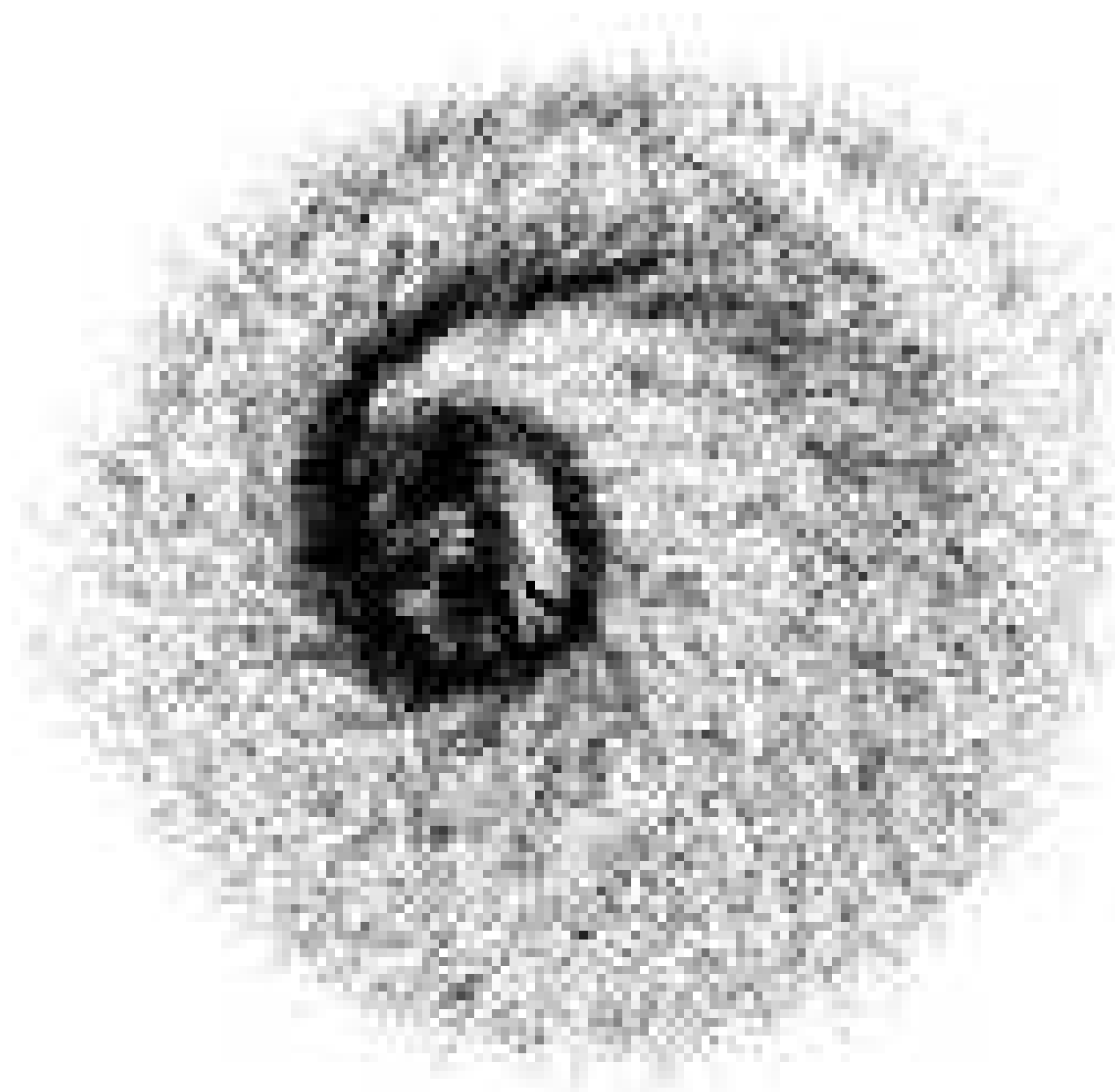


Fig. 21a.—



Fig. 21b.—



Fig. 21c.—

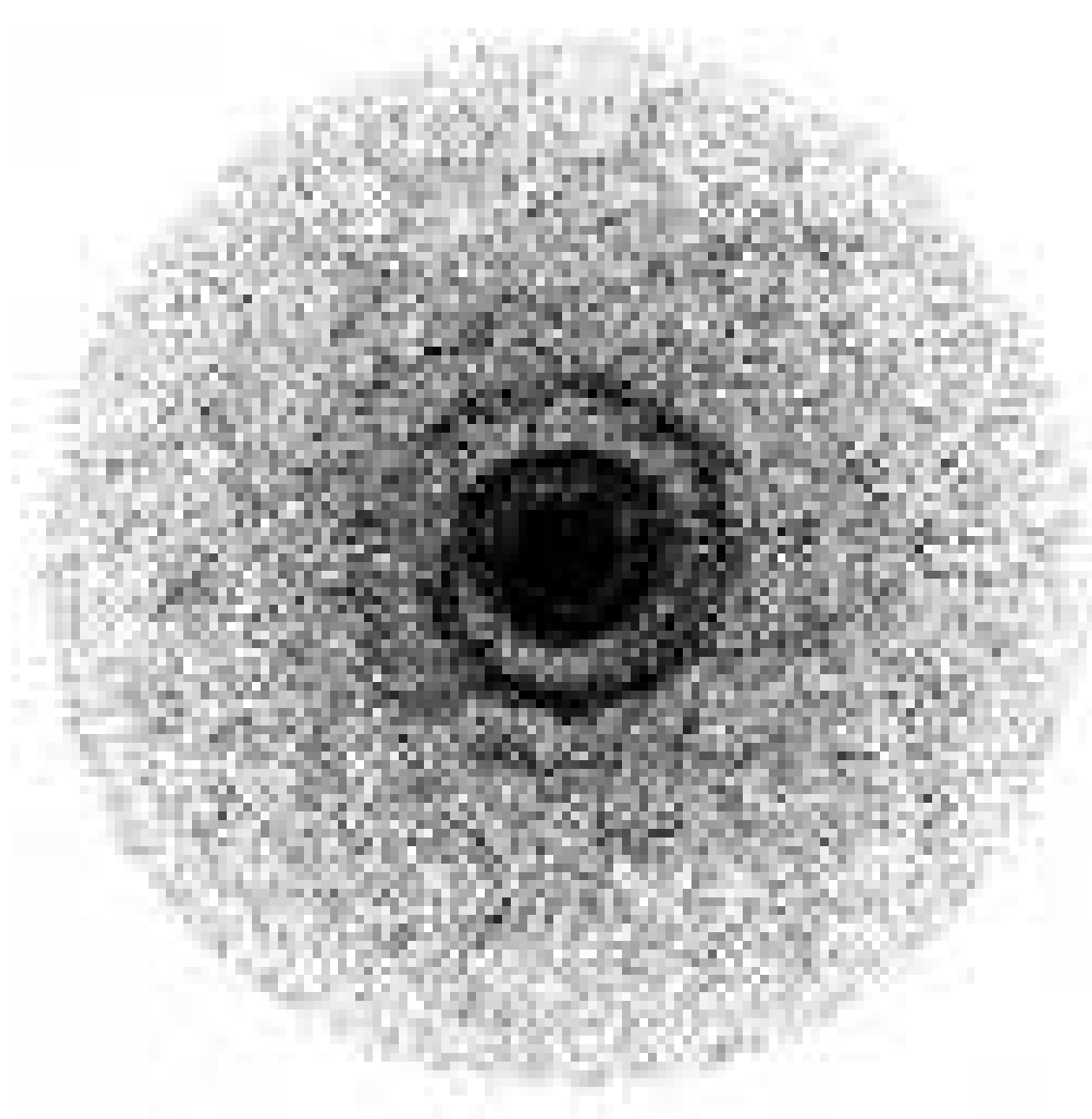


Fig. 22a.—

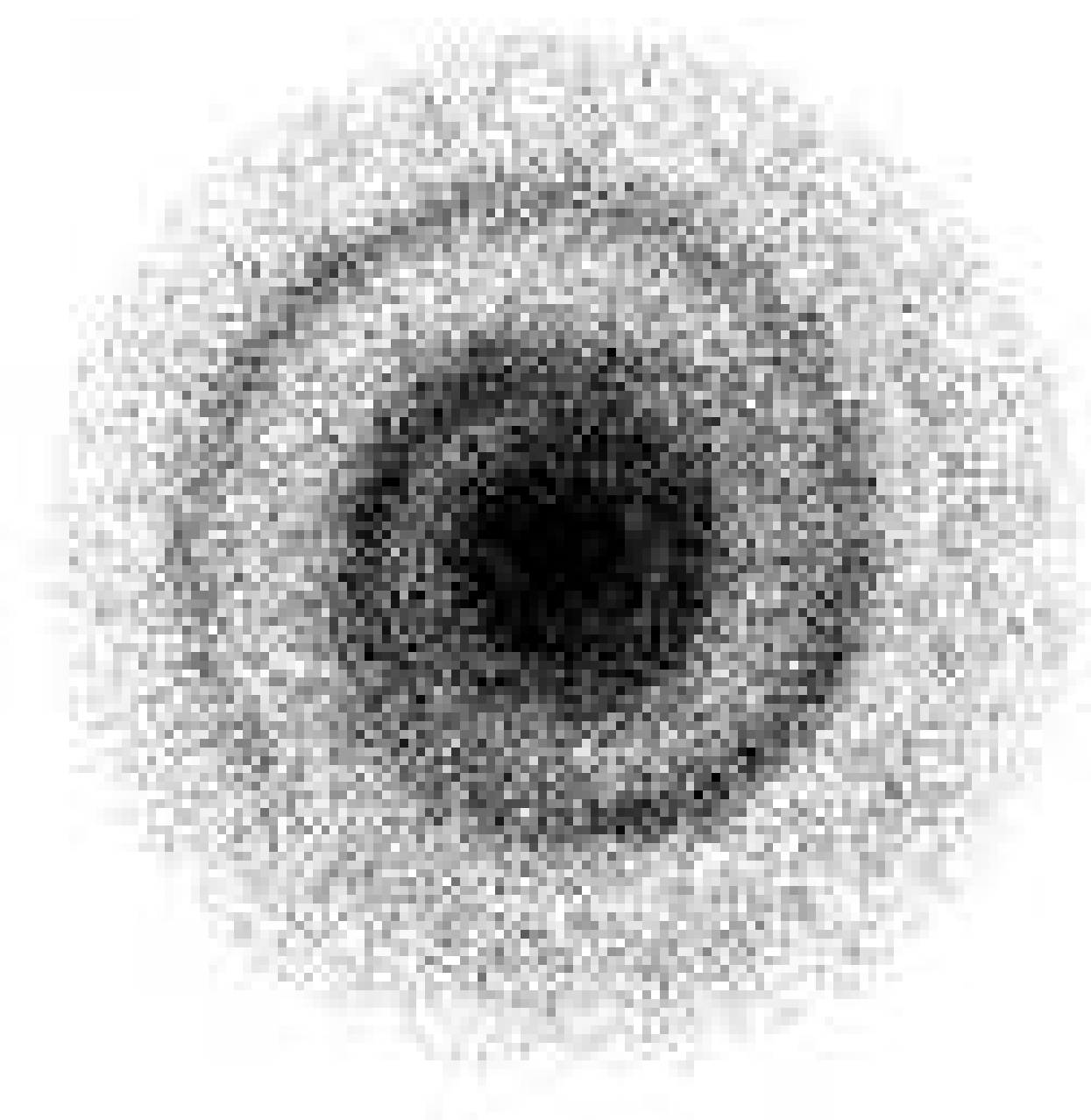


Fig. 22b.—

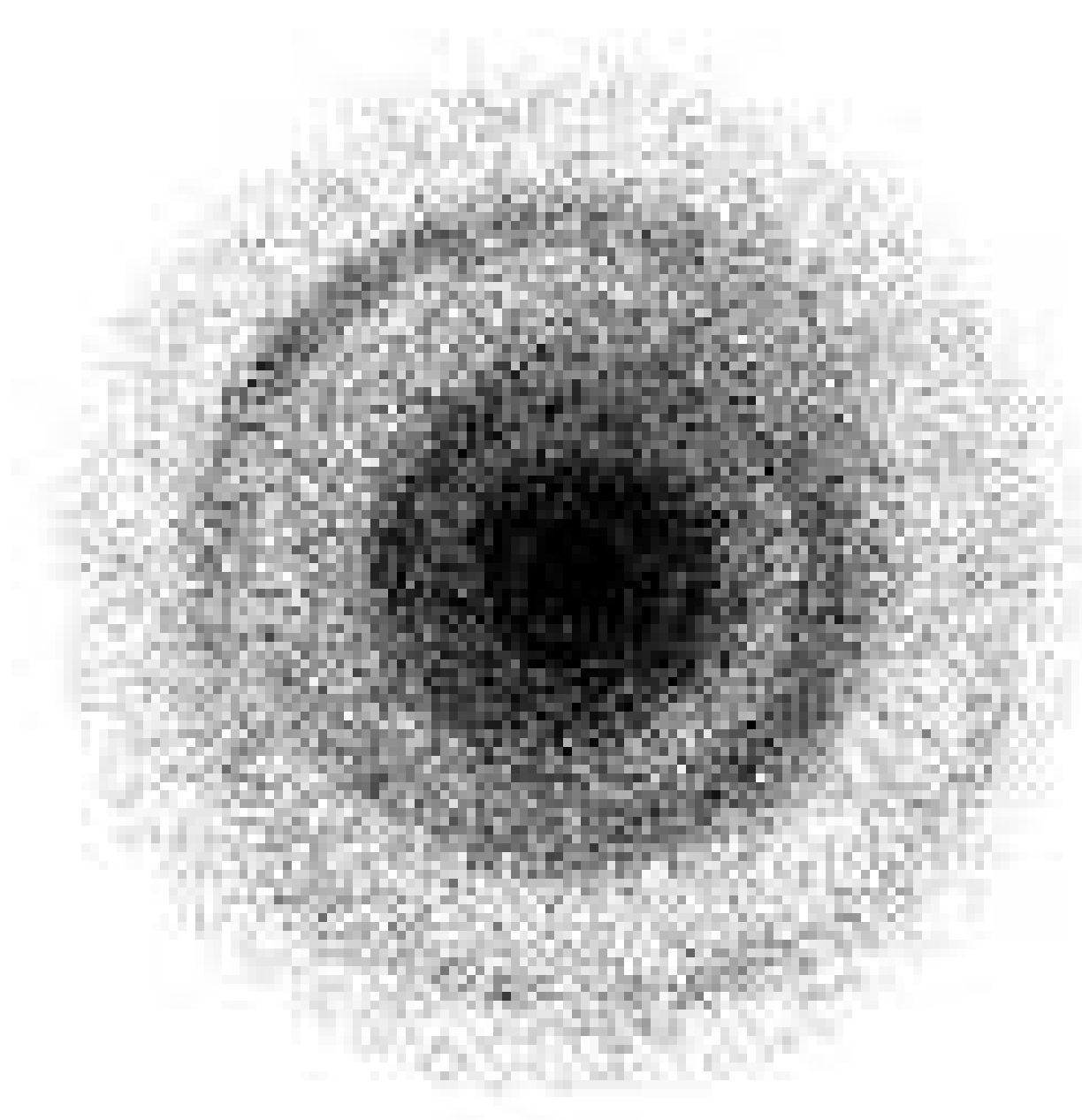


Fig. 22c.—

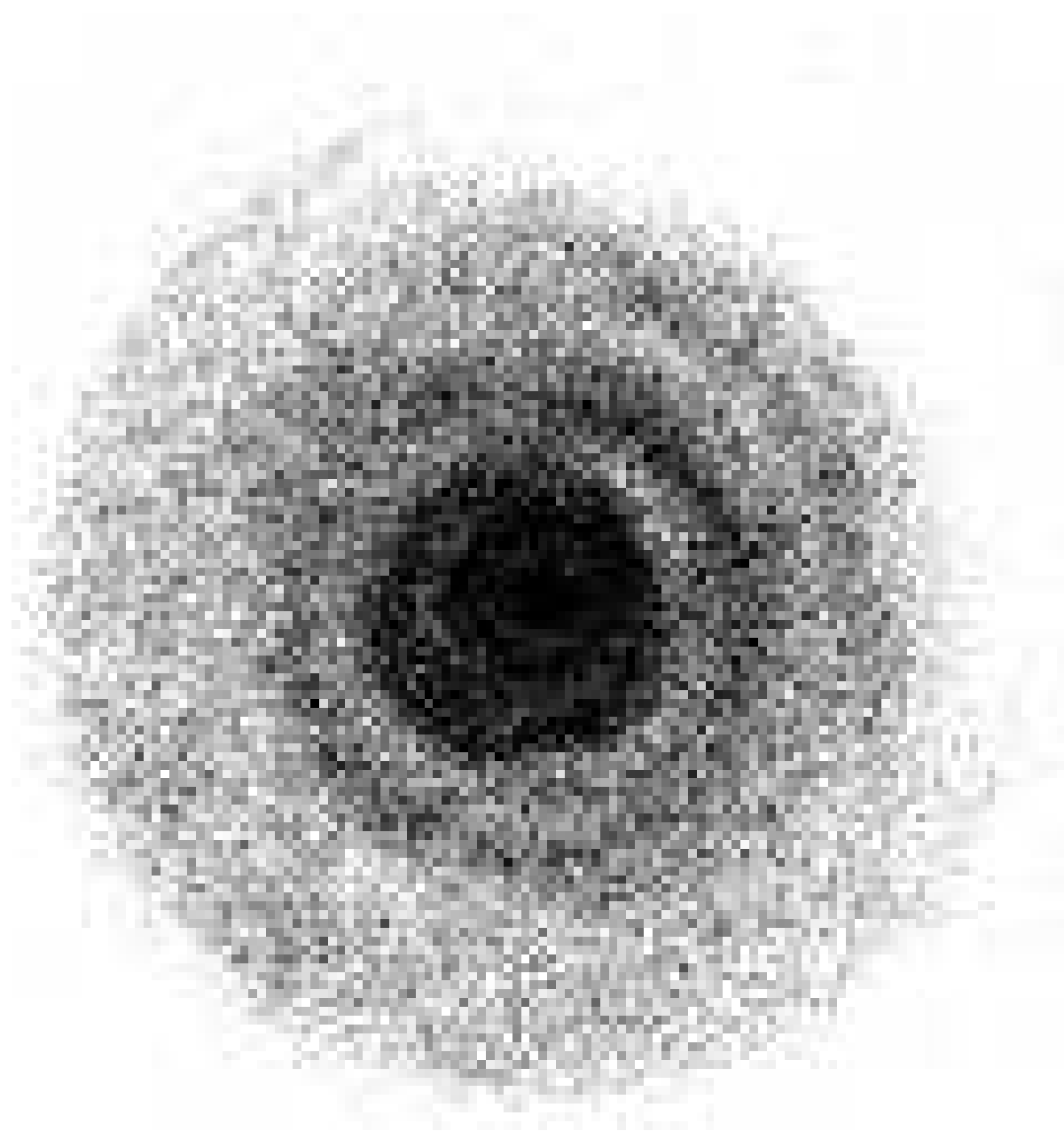


Fig. 23.—



Fig. 24.—